Using species distribution models to inform seasonal closures - minimizing river herring and shad catch in the Atlantic herring fishery

Prepared for the Atlantic Herring Plan Development Team (PDT) by
Micah Dean and Ben Gahagan, Massachusetts Division of Marine Fisheries

Submitted to the New England Fishery Management Council by the Atlantic Herring PDT
November 10, 2026

Introduction

Anadromous alosines (e.g., alewife, blueback herring, American shad, hickory shad – referred to hereafter collectively as 'river herring and shad', or RHS) frequently intermix with Atlantic herring during their ocean habitation phase along the Northeast US coastal shelf (Cournane et al., 2013; Bethoney et al., 2014). Consequently, the unintended catch of these RHS species in the Atlantic herring fishery has been a concern of fishery managers for decades (Kritzer et al., 2022), particularly given the general coastwide decline in RHS populations (Hare et al., 2021). Framework Adjustment 3 to the Atlantic Herring Fishery Management Plan (FMP) implemented the current regulatory approach to minimize RHS catch in the fishery through gear and area-specific caps on the amount of RHS that can be caught each year (Figure 1; RHS 'catch caps' - NEFMC 2014, 2016). Due to the anadromous life history and distributed stock structure of RHS populations (i.e., philopatry leads to each river functioning as its own demographic stock), coastwide analytical stock assessments do not exist for this complex of species (ASMFC 2024). Consequently, there are no comprehensive estimates of total biomass, mortality rates, or reference points from which biologically-based RHS catch caps can be set (i.e., at a sustainable level that does not compromise population productivity). Lacking a biologically-based reference point, the NEFMC set catch caps at the average of annual RHS catch estimates from a reference period (2008-2014), with the stated objective of providing a strong incentive for the fishery

to continue to avoid RHS and reduce RHS catch to the extent practicable (NEFMC 2014). Other than some minor changes to how the average of the reference period was calculated, cap amounts have remained unchanged since implementation (NEFMC 2024). Although the plan includes a secondary objective to allow for future adjustments in cap amounts as more information becomes available, no exact process was established due to the lack of RHS population metrics.

Since they were enacted, RHS catch caps have triggered an area closure on four occasions. These events resulted in between 13,000 to 201,000 km^2 of lost access for the Atlantic herring fishery for 8 to 11 months per year (i.e., 0.1 to 1.8 million km^2-months). Due to low observer coverage rates for this fishery (often < 10%), each of these closures were based on very few observations (≤ 5 trips) and estimated RHS catch rates were highly uncertain (often with CV > 1.0). In all but one case, coverage rates were so low that observations from the prior year had to be included in the calculation of the RHS catch rate. Given this past performance, it appears that the current system is susceptible to triggering broad closure events based on limited information, imposing significant costs on the fishery. Due to federal funding cuts to NOAA, the capacity to monitor fishery catches has been further curtailed, which will result in less data and greater uncertainty in future RHS catch estimates.

There are several drawbacks to the current system of static catch caps based on a reference period: 1) we do not know if the level of RHS catch from the reference period is sustainable; 2) the relative amount of protection afforded to RHS species decreases as their populations decline, or the Atlantic herring quota declines; 3) a substantial amount of in-season fishery monitoring and communication is required; 4) large closures can be triggered by uncertain estimates derived from a small number of samples; 5) RHS catch rates are assumed to be similar across very large areas (Figure 1).

By design, this system intends to incentivize fishing captains to avoid catching RHS and assumes they possess sufficient knowledge of RHS distributions to do so. However, through this avoidance, fishing captains gain fewer relevant observations over time, weakening this ecological knowledge. Other factors, such as increasing fuel prices (Conley et al., 2026) and declining catch limits for Atlantic herring (NEFMC, 2025) have further restricted fishing effort, which leaves large knowledge gaps for fishing captains seeking to avoid RHS. Fortunately, other data sources exist to help inform the distribution of RHS species. Multiple fishery-independent trawl surveys operate annually along the Northeast US coastal shelf, each designed to provide an unbiased description of fish abundance. Although substantial differences exist between these surveys (e.g., net design, towing protocol, survey seasons and areas), their datasets can effectively be integrated to provide

a single comprehensive description through a *species distribution model* (Paradinas et al., 2023).

Multiple research groups have developed species distribution models to predict times and areas of high RHS catch in the Atlantic herring and mackerel fisheries (Bethony et al., 2014; Turner et al., 2016, 2017; Roberts et al., 2023). Although each has demonstrated that RHS distributions are predictable in time and space, their focus to date has been on improving the performance of the catch cap system by providing timely forecast information to the fishery. As such, none of these approaches have addressed the underlying issues with the current system.

Here, we propose a different approach to the use of species distribution models for avoiding RHS in the Atlantic herring fishery. Given the predictability of RHS populations, we aim to identify areas and seasons where RHS are consistently abundant over time. We then plan to use these patterns to inform the development of fixed seasonal closed areas that could replace the catch cap system. Doing so would address each of the major drawbacks of the current system by providing consistent protection through targeted closures that prevent the need for biological reference points or in-season monitoring.

Methods

The overall approach (see Figure 2 for a conceptual diagram) was to first assemble all known observations of RHS catch-per-unit-effort (CPUE) to provide the most comprehensive dataset possible of their spatial and seasonal distribution. Species distribution models were fit to these data, accounting for the influence of environmental predictors as well as residual spatial patterns. These models were then used to make general monthly predictions of the spatial distribution of each population during their oceanic residency. Finally, predicted monthly RHS distributions were used to structure a series of hypothetical closed area scenarios that offer various points along the tradeoff continuum between RHS protection and access for the Atlantic herring fishery. These scenarios were evaluated by comparing the closure boundaries to the distribution of past RHS and Atlantic herring catches in the directed Atlantic herring fishery. As a further point of comparison, a species distribution model was also constructed for Atlantic herring to provide a comprehensive account of their spatial and seasonal distribution.

Datasets

Data from 9 scientific bottom trawl surveys were assembled to inform the development of species distribution models (Table 1). These surveys were selected because they provide standardized and precise measures of catch (in kg), effort (area

swept in km^2), and location (lat/lon of tow midpoint) within the range of RHS species and the Atlantic herring fishery. Although some surveys conduct many "cruises" (i.e., a complete sampling of the survey domain) throughout the year, most are limited to 2 just cruises that represent "spring" and "fall" (Figure 3). Collectively, these survey datasets provide broad spatial coverage of the Northeast US coastal shelf, particularly during the spring and fall survey windows (Figure 4). Although some survey datasets extend as far back as 1963, many began collecting data in the 1980s and 1990s. Therefore, all analyses were restricted to the period 2000-2023, when most surveys were operational.

To further expand the seasonal coverage of observations, the trawl survey dataset was augmented with records from NOAA Fisheries' Northeast Fisheries Observer Program (NEFOP or Observer Program). Similar to trawl surveys, fishery observers record standardized measures of catch, effort, and location by haul and have reliable species identifications. Observer data were assembled for two of the three primary gear types used in the Atlantic herring fishery: small-mesh bottom trawl (SMBT; cod-end mesh size < 4") and midwater trawl (MWT). Purse seines, the other primary gear type, are primarily used in Management Area 1A (inshore Gulf of Maine) to target individual monospecific schools of herring (Figure 1), and generally have very little catch of RHS (Benaka et al., 2019). As such, purse seines were excluded from the analyses presented here. SMBT and MWT fishery observations were not filtered by target or landing species, to include any trip that was *capable* of catching both RHS and Atlantic herring. The average of the start and end haul coordinates were used to represent the haul location. Area swept by haul (in km^2) was estimated as follows: First, linear models were fit to NEFOP records where net width and footrope length were available, by gear type. These models were then used to predict net width from footrope length for any record where net width was unavailable. Area swept was then calculated as the product of estimated net width, tow speed, and tow duration.

The catch per unit effort (CPUE) was used as the response variable in all models and was calculated by dividing the recorded catch weight (kg) by the area swept (km^2) of each haul. Any non-standard hauls that had recorded issues with the fishing performance of the gear (e.g., hangs, tears, etc.) were omitted from the dataset. Several environmental variables were included as potential predictors of RHS abundance, including depth, surface temperature, bottom temperature, surface salinity, and bottom salinity. When environmental data were unavailable for a haul, auxiliary datasets were used to impute a value, given the haul date, time, and location: depth – Generalized Bathymetric Chart of the Oceans (GEBCO; Weatherall et al., 2015); temperature and salinity – Finite Volume Community Ocean Model (FVCOM; Chen et al., 2006). Prior to model fitting, a random 10% subset of the dataset was reserved for testing model predictions. All models were fit to the remaining 90% of observations.

Species Distribution Models

Species distribution models were fit to the combined trawl survey and fishery observer dataset for each species separately. Although hickory shad are included in RHS catch caps, there is far less information available from which to describe the distribution of this species (percent occurrence in the NEFSC survey is very low at 0.08%); as such, all models, predictions, and closure scenarios were built from data on the remaining three RHS species (alewife, blueback herring, and American shad), as well as for Atlantic herring. The *sdmTMB* package (Anderson et al., 2025) of the R statistical software (R Core Team, 2024) was used to develop all models, while the *terra* package (Hijmans et al., 2022) was used for all other spatial manipulation and analysis. The *sdmTMB* framework utilizes Gaussian Markov spatial random fields to account for residual spatial patterns, and was found to outperform other approaches (GAMs, Random Forest) during initial testing. The *sdmTMB* implementation of spatial random fields uses a triangular mesh (as opposed to a continuous surface across the spatial domain), which vastly decreases computation time and allows for logical interpolation around complex shorelines (Bakka et al., 2019).

Prior to model development, the delta-lognormal distribution was selected as the most appropriate error distribution by fitting a range of statistical "families" to a naïve *sdmTMB* model (i.e., CPUE ~ 1; intercept only). As a type of "hurdle" model, the delta-lognormal distribution is the product of a binomial distribution, representing the probability of occurrence, and a lognormal distribution for the positive values, resulting in two sub-models for each species. Delta-lognormal models are often the best choice for describing the relative abundance of schooling pelagic fish species because their datasets are often zero-heavy and positive observations have a long right tail (Lo et al., 1992).

Candidate predictors included three different temporal variables: YEAR, day-of-year (J), and hour-of-day (H) (Table 2). Environmental predictors included both static variables, such as DEPTH and distance from shore (DSHORE), and dynamic variables, such as temperature (BOTTEMP, SURFTEMP) and salinity (BOTSALIN, SURFSALIN). Dataset SOURCE (i.e., survey platform, or fishery gear type) was treated as a factor to account for differences in catchability. Smoothers (i.e., s(*X*)) were used for each continuous variable, given that fish species typically have non-linear relationships with environmental variables (Anderson et al., 2022). 2D smoothers were also evaluated for each continuous variable, which allowed the non-linear functions to vary seasonally (i.e., s(*X*, J)). To prevent overfitting of data and decrease the computational cost of model fitting (Wood, 2017), the maximum basis dimension (k) was set to 3 for 1D smooths and 9 for 2D smooths. Finally, the spatial random field was allowed to vary over time, either by YEAR or MONTH.

Model development followed a sequential process that was intended to minimize the time required to fit and select a 'best' model for each species:

1) A moderately coarse (n = 150 knots) triangular mesh (Figure 5) was established for the spatial random field, encompassing the entire domain of all observations. Denser meshes significantly increase computation time and do not always result in more accurate predictions (Ward and Anderson, 2025).
2) Environmental predictors were selected via forward selection from the suite of candidate variables (Table 2) using the Bayesian Information Criterion (BIC), which is less likely to result in overfitting, improving the out-of-sample predictive skill for models fit to large datasets (Warren and Seifert, 2011). The same environmental predictors were kept for both the binomial and lognormal model components, which is a requirement of the *sdmTMB* framework (Anderson et al., 2025).
3) Once the main environmental predictors were selected, the spatial random field was allowed to vary over time either by year or by month, following a 1st-order autoregressive process (AR1). The spatiotemporal form that resulted in the lowest BIC was selected. By selecting environmental predictors first, the spatiotemporal random field is prevented from unduly absorbing variation that could otherwise be described by fixed effects (Davies et al., 2023).
4) After the best environmental predictors and spatiotemporal forms were selected, each model was re-fit using a denser triangular mesh (n = 300 knots), allowing for higher resolution predictions. Progressing from moderate mesh resolution during model selection to higher resolution during final model fitting is considered standard workflow when developing *sdmTMB* models (Anderson et al. 2026).

The prediction skill of each species distribution model was evaluated using the reserved 10% out-of-sample test dataset. Specifically, the observed log(CPUE) and %-occurrence of the test records were plotted against the predicted values, grouped by 10% quantile bins. An increasing relationship between observed catch rates (i.e., occurrence and/or CPUE) and predicted densities suggests that the models are able to successfully predict RHS distributions from new data that weren't used to train the model.

Predicted Distributions

To make use of the species distribution models for creating seasonal closed areas, average monthly predictions were made across the entire model domain. Although *sdmTMB* models are fit using a triangular mesh, it is more convenient to make predictions according to a regular raster grid with consistent horizontal and vertical resolution. This was accomplished through barycentric interpolation, wherein predictions at a grid point are made via an average of the vertices of the mesh triangle encompassing that point,

weighted by the distance to each vertex (Lindgren et al., 2011). All model predictions presented here were made at locations defined by a raster grid with 2500 m resolution, encompassing coastal shelf waters between the US-Canada border and Cape May, NJ. Grid locations were then replicated for each month and year between 2000 and 2023. The depth at each grid location was extracted from the GEBCO model, while the mean temperature and salinity values were extracted from the FVCOM model at each grid location, year, and month. The fitted models were then used to predict the density of each species at all grid locations for each year and month. For each grid location, density predictions were averaged across years by month, yielding 12 predicted rasters for each species, representing average monthly distribution over the past two decades. To help communicate distribution patterns, the average predicted density for each species was calculated for groups of NOAA statistical reporting areas, by month.

Monthly rasters for alewife, blueback herring, and American shad were added together to create a series of rasters representing the seasonal distribution of RHS species in aggregate. To augment interpretability, these aggregate RHS rasters were then converted from predicted densities (kg/km2) to biomass quantiles. To accomplish this, predicted values at each grid location and across all months were sorted in decreasing order, and a cumulative sum was calculated for each record. These cumulative values were then divided by the sum of all values. This ultimately created a set of monthly rasters where the values represent the quantile of RHS biomass throughout the year, which is akin to how a utilization distribution is derived from telemetry datasets (Millspaugh et al., 2006). As an example, raster regions with biomass quantile values greater than 0.7 represent the minimum area that encompasses 30% of the predicted RHS biomass throughout the year.

The relevance of these RHS biomass quantile rasters to actual fishery catch rates was assessed by comparing the %-occurrence and log(CPUE) of each species from all observed fishery hauls (by gear type) to the predicted raster values, grouped into 10% quantile bins. An increasing relationship between fishery catch rates (i.e., occurrence and/or CPUE) and RHS raster values suggests the approach is informative for predicting fishery catches and would be relevant to the design of seasonal closed areas.

Closure Scenarios

It is unrealistic to establish seasonal fishery closures directly from SDM output at 2500 m resolution, given that communication and enforcement of area boundaries would be a significant challenge (i.e., requiring thousands of coordinate pairs). Therefore, an algorithm was created to delineate closure boundaries that encompass the primary RHS areas while decreasing the complexity of the resulting polygons (i.e., with only a small number of coordinate pairs). After selecting a minimum biomass quantile (q_{min}), a set of

points was created from all the grid cells that met this condition, for each month. Concave hull polygons (Asaeedi et al., 2017) were then created to enclose these points, using a concavity threshold of 0.5 (where 0 = the tightest bounds and the greatest number of vertices, and 1 = the loosest bounds and the least number of vertices). This algorithm sometimes resulted in multiple polygons per month when more than one distinct patch of grid cells were selected. To avoid unnecessary complexity that offered little additional RHS protection, patches of grid cells under 100 km^2 were ignored when creating closure boundaries.

Closure alternatives were evaluated using all fishery observer records from 2000-2022 for SMBT and MWT gears, where Atlantic herring were kept. From these data, we calculated the mean CPUE of RHS and Atlantic herring inside and outside of the hypothetical closed areas, as well as the fraction of total observed RHS and Atlantic herring catch encompassed by closed areas. Although we also constructed a model for Atlantic herring that describes their seasonal distribution along the entire coastal shelf, such information is insufficient to inform expectations about where and when the fishery is likely to operate. A captain's decision on where to fish is a complex balancing act that integrates multiple factors, including overhead costs (e.g., fuel, distance from port), regulations (e.g., available quota, trip limits, closed areas, disincentives to make exploratory tows), and the environment (e.g., depth, weather patterns), in addition to prior knowledge of resource abundance (i.e., density of Atlantic herring). As such, we felt that past fishing patterns were a more effective choice for evaluating closure scenarios than the predicted distribution of Atlantic herring. However, depending on the gear type and time of year, a significant fraction of the coastal shelf may already be unavailable to the Atlantic herring fishery due to various existing regulations (Figure 6). Therefore, the evaluation dataset was further restricted to just the times and areas that are currently open to fishing for a given gear type.

Results

Species Distribution Models

The selected models for all species included terms for both SOURCE and YEAR (Tables 2 and 3), which acknowledges that catchability varies significantly across datasets and that the general abundance of these populations fluctuates over time. The marginal year effects suggest that each RHS species had a generally increasing trend from 2000-2019, but a flat or declining trend in recent years (2020-present) (Figures 7-9). Atlantic

Herring showed a trend that was initially flat, increasing from 2005-2011, and then declining from 2012 onward (Figure 10).

Each species exhibited a different relationship with the environmental variables of depth, temperature, and salinity (Figures 7-10). Alewife showed a general preference for depths deeper than 100m, bottom temperatures between 10° and 15° C, and were more frequently encountered in low salinity areas in springtime. Blueback herring preferred depths between 100 and 200 m and surface temperatures near 15° C. American shad were associated with depths >150 m, particularly outside of summer months, and had a weak association with cooler surface temperature. Atlantic herring were generally associated with cooler bottom and surface temperatures (<15° C) and were most abundant at depths < 150 m.

The residual spatial pattern of each species was best explained by continuous seasonal variation (AR1 by month), as opposed to interannual variation (i.e., AR1 by year), providing support for spatial distributions that persist across years (Table 3). Interestingly, each species showed a seasonal decrease in overall abundance during summer-fall (day of year 200-300). There was a clear positive relationship between observed values (both CPUE and occurrence) and predicted density from the test dataset, suggesting the models are able to predict the distribution of each species from unseen data (Figure 11). This positive relationship was evident for all species and across all seasons, years, and management areas.

Predicted Distributions

Alewife were concentrated near Rhode Island in January and February (Figures 12 and 16). The distribution moved northward to outer Cape Cod, Georges Bank, and the coast of Maine by April and May. Alewife were generally less abundant in summer months, except for eastern Maine. Abundance increased again in the fall as the population became concentrated along the western Gulf of Maine coast from Maine to Massachusetts and then transitioned back to southern Massachusetts and Rhode Island by December.

Blueback herring showed a somewhat similar seasonal pattern to alewife, only shifted farther south (Figures 13 and 16). From January through May, they were concentrated off New Jersey and New York (south of Long Island), as well as near Rhode Island and outer Cape Cod. The distribution shifted northward in June to the southwestern Gulf of Maine, from Cape Cod Bay (Massachusetts) to Casco Bay (Maine). Blueback herring were less abundant in the model domain during the summer months, with pockets of abundance along the northern Massachusetts shoreline. Abundance increased again in

October and as Fall progressed the distribution extended southward to include southern Massachusetts in November and then Rhode Island in December.

American shad were less abundant but more widely distributed than the other two RHS species (Figures 14 and 16). In January, there were several pockets of abundance, including Long Island Sound, outer Cape Cod, offshore Maine, and along the shelf edge south of New England. By April and May, they became concentrated along the New Jersey and New York coastline, offshore of southern New England, and on Georges Bank. They moved northward in summer and became most abundant along the Maine coast from June through September. Their distribution then extended southward to include northern Massachusetts in October and southern Massachusetts, Rhode Island, and Long Island Sound in November and December.

Atlantic herring were primarily found in off Rhode Island and into Long Island Sound from December through February, transitioning farther south in April to the Hudson Canyon area off New York and New Jersey (Figures 15 and 16). From May through July, this pattern shifted northward to pockets of abundance along the northern edge of Georges Bank and eastern Maine. From August through November, Atlantic herring were abundant in patches along the Maine, New Hampshire, and northern Massachusetts coastlines, as well as along the northern edge of Georges Bank.

When the three RHS species were combined into a single set of monthly rasters and converted to biomass quantiles, patterns originating from each species' distribution could still be discerned (Figure 17). However, given the greater predicted abundance of alewife, that species has the greatest influence on the overall distribution of RHS biomass. Regardless, there is a strong positive association between the predicted RHS biomass quantile and both the occurrence and abundance of each RHS species in the observed fishery hauls (Figure 18).

Closure Scenarios

Each of the evaluation metrics showed a wide range of results with respect to closure scenarios derived from the minimum RHS biomass quantile rasters (Figure 15). At the lowest quantile (q_{min} = 0.1), 99% of the observed RHS catch for both midwater trawl and bottom trawl was encompassed by the closure (Figure 19; Table 4). However, the scale of closures under this scenario was expansive, encompassing the majority of the observed Atlantic herring catch (50% for midwater trawl; 99% for bottom trawl). Only midwater trawl landings from June-October on Georges Bank would remain open to the fishery. In contrast, the closure scenario based on the highest quantile (q_{min} = 0.9) would have prevented just 9% of the bottom trawl RHS catch and 22% of the midwater trawl RHS catch. In this case,

closures would be very limited in space and time, and have minimal impact on access to Atlantic herring (preventing 3-4% of the observed catch of Atlantic herring). The range of alternatives between these two extreme scenarios provide intermediate levels of RHS protection and access to Atlantic herring.

Discussion

There is a clear tradeoff between protection of RHS species and fishery access to Atlantic herring - when protection for RHS is increased, the fishery loses access to Atlantic herring. As an alternative to catch caps, we have developed a system of seasonal area closures that optimize this tradeoff by prohibiting fishing in only the specific times and locations where RHS are consistently abundant. By utilizing species distribution models derived from 80,000+ standardized observations, we were able to take advantage of the subtle differences in how Atlantic herring and RHS species relate to their environment. The scenarios presented here could provide consistent meaningful protection to RHS while excluding the Atlantic herring fishery from a relatively small area (e.g., <0.09 million km^2-months, when q_{min} = 0.7), as compared to past catch cap closures (>1.8 million km^2-months). It is worth noting that the closure scenarios presented here are only hypothetical examples. Multiple elements of their design could be varied to create alternatives for managers to select from. For instance, the minimum biomass quantile (q_{min}) provides a continuum of choices for the tradeoff between RHS protection and access to Atlantic herring fishing (Table 4). The complexity of area boundaries can be controlled via the concavity threshold when using concave hull polygons to delineate closures (Figure 20). Although we presented only monthly closure scenarios, alternatives could be considered that vary less frequently (e.g., bi-monthly, quarterly). Regardless of the specific configuration, it is important that each scenario be linked to the patterns described by the species distribution models, which ensures that RHS conservation is provided efficiently (i.e., prohibiting fishing in only the most important times and areas).

A key aspect of using species distribution models to design seasonal closed areas is the spatial persistence of distributions across years. The current system of RHS catch caps relies on the inherent assumption that areas of high RHS catch are unpredictable, necessitating continuous in-season monitoring of RHS catch rates, by gear and area. In contrast, we found no support for interannual variation in spatial pattern in any of the species' models (beyond what could be explained by environmental covariates), suggesting that their distributions are predictable in future years. The ability of the models to predict RHS distributions from unseen data was validated by demonstrating a clear

positive relationship between predicted and observed values from the test dataset (Figure 11). Although YEAR was included in the selected models as a random intercept, this only accounted for interannual variation in population size and did not impact their spatial distributions.

Despite our finding of persistent spatial patterns for RHS species, it is still possible that their distributions might shift over time due to their associations with water temperature. However, the *seasonal* variability in ocean temperature is much greater than the multi-decadal trend associated with climate warming (Bulgin et al., 2020). As such, the models presented here, which fully capture seasonal patterns, will likely be relevant for many years to come. If the NEFMC were to adopt a model-based closure system, we recommend occasionally reevaluating the closure boundaries with new survey and observer data, according to a regular cycle (e.g., every ten years).

Previous distribution models to inform Atlantic herring fishery management have also demonstrated that RHS distributions are predictable in time and space (Turner et al., 2016, 2017; Roberts et al., 2023). However, there are some important distinctions between previous work and the models presented here. These earlier studies were fit to only the NEFSC bottom trawl survey dataset, which lacks the extensive seasonal and spatial coverage provided by the collection of surveys and fishery-dependent observations assembled here. Furthermore, by focusing on occurrence (i.e., presence/absence) as the response variable, they were unable to account for the variation in RHS *abundance*, which is ultimately the driver of catch rates. Both Turner et al. (2016, 2017) and Roberts et al. (2023) used Generalized Additive Models (GAMs) that accounted for environmental influences via non-linear smoothers, which is equivalent to how we handled such fixed effects via the *sdmTMB* framework. However, *sdmTMB* and other related model types (e.g., VAST, INLA) offer the added benefit of accounting for residual spatial pattern via Gaussian Markov Random Fields. Most animal populations exhibit persistent residual spatiotemporal patterns that cannot be explained by measured environmental variables. Consequently, distribution models like *sdmTMB* that incorporate spatiotemporal random effects often drastically outperform models that only account for fixed environmental effects (i.e., GAMs) (Thorson et al., 2015, 2019; Brodie et al., 2020; Anderson et al., 2025).

Our results show that most of the past midwater trawl catch of RHS could have been avoided by prohibiting access to a relatively small amount of the past Atlantic herring catch (e.g., 69% of RHS catch and 19% of Atlantic Herring catch, when $q_{min} = 0.7$). It appears that the distribution of midwater trawl landings of Atlantic herring includes many times and areas where RHS are not concentrated (e.g., Georges Bank). However, lost access to herring fishing grounds may be more problematic for the midwater trawl fleet,

given that it primarily targets just Atlantic herring (and sometimes mackerel). In contrast, past catches of RHS and Atlantic herring are far more coincident in the small mesh bottom trawl fishery, making it difficult to identify closure scenarios that do not also prevent access to Atlantic herring (e.g., 58% of RHS catch and 57% of Atlantic herring catch were encompassed, when q_{min} = 0.7). This was caused by the relatively narrow footprint of the SMBT landings of Atlantic herring – near Rhode Island in Winter, and from Cape Ann, MA to New Hampshire in Summer – both times and areas that hold concentrations of RHS.

Accounting for the multi-species nature of the SMBT fishery may be important for the success of any regulation designed to minimize RHS catch under the Atlantic herring FMP. In our efforts to evaluate the hypothetical closure scenarios, we chose to define an "Atlantic herring trip" as any observed trip where Atlantic herring were reported kept on at least one haul, which should include all trips where vessels "declared" into the Atlantic herring fishery via the pre-trip notification system, as wells as trips made by vessels that are not required to make such declarations (i.e, Category D). We did not choose to limit trips by a minimum amount of Atlantic herring landings (e.g., 2000 or 6600 pounds have been used in other aspects of the fishery management plan), because we wanted to account for the full tradeoff between protection of RHS species and participation in the Atlantic herring fishery. However, SMBT vessels that plan to target squid, butterfish, and/or whiting can declare "out-of-fishery" for Atlantic herring, which means they would not be subject to seasonal area closures defined under the Atlantic herring FMP. Therefore, SMBT trawls could continue to operate in areas with high abundance of RHS species.

The models presented here were intended to account for the distribution of anadromous RHS species during their oceanic phase. This ignores a substantial portion of their life history, because reproductive adults are in riverine habitats during the spring spawning period and are therefore unavailable to bottom trawl surveys and ocean fisheries. Interestingly, none of our models detected a large springtime decrease in abundance, which may be due to the overwhelming abundance of immature and sub-adult fish in the ocean, given that RHS species typically take 3-6 years to reach maturity (Brown et al., 2025). Instead, each species showed a general decline in ocean abundance during the summer months (Figures 7-10). Monthly predicted distributions indicated high densities toward the northern edge of the model domain from late spring through early fall (Figures 12-16), suggesting that a portion of each population may spend the summer in Canadian waters. Multiple tagging and demographic studies support the idea that RHS species transit the US-Canada border during summer months (Leggett 1977; Rulifson and Dadswell, 2020; Gahagan and Bailey, 2020).

In summary, this paper outlines a viable alternative to the current approach for minimizing RHS catch in the Atlantic herring fishery. By creating seasonal closed areas based on species distribution models, managers could avoid several of the drawbacks of the current catch cap system: 1) There is no need for analytical stock assessments (which do not exist) to identify an appropriate and sustainable catch limit for RHS species; 2) Constant in-season monitoring of fishery RHS catch rates is not required, and closures would no longer be triggered by a small number of highly variable observations; 3) The relative amount of RHS protection and lost fishing access to Atlantic herring would not fluctuate with the size of RHS populations and/or the Atlantic herring quota; 4) The expanse of the area closures would be limited to only those times and areas most important for RHS conservation.

References

Anderson, M.J., Walsh, D.C., Sweatman, W.L. and Punnett, A.J., 2022. Non-linear models of species' responses to environmental and spatial gradients. *Ecology Letters*, *25*(12), pp.2739-2752.

Anderson, S.C., Ward, E.J., English, P.A., Barnett, L.A. and Thorson, J.T., 2025. sdmTMB: an R package for fast, flexible, and user-friendly generalized linear mixed effects models with spatial and spatiotemporal random fields. *Journal of Statistical Software*, *115*, pp.1-46.

Anderson, S.C. Ward, E.J., English, P.A., Barnett, L.A., and Thorson, J.T., 2026. Introduction to modeling with sdmTMB. Vignette for sdmTMB R package, version 1.1.0.9032.

Asaeedi, S., Didehvar, F. and Mohades, A., 2017. α-Concave hull, a generalization of convex hull. *Theoretical Computer Science*, *702*, pp.48-59.

Atlantic States Marine Fisheries Commission (ASMFC). 2024. River herring benchmark stock assessment and peer review report. pp 1-499.

Bakka, H., Vanhatalo, J., Illian, J.B., Simpson, D. and Rue, H., 2019. Non-stationary Gaussian models with physical barriers. *Spatial statistics*, *29*, pp.268-288.

Benaka, L.R., D. Bullock, A.L. Hoover, and N.A. Olsen (editors). U.S. National Bycatch Report First Edition Update 3. 2019. U.S. Dept. of Commerce, NOAA. *NOAA Technical Memorandum* NMFS-F/SPO-190, 95 p.

Bethoney, N.D., Stokesbury, K.D. and Cadrin, S.X., 2014. Environmental links to alosine at-sea distribution and bycatch in the Northwest Atlantic midwater trawl fishery. *ICES Journal of Marine Science*, *71*(5), pp.1246-1255.

Bulgin, C.E., Merchant, C.J. and Ferreira, D., 2020. Tendencies, variability and persistence of sea surface temperature anomalies. *Scientific reports*, *10*(1), p.7986.

Brodie, S.J., Thorson, J.T., Carroll, G., Hazen, E.L., Bograd, S., Haltuch, M.A., Holsman, K.K., Kotwicki, S., Samhouri, J.F., Willis-Norton, E. and Selden, R.L., 2020. Trade-offs in covariate selection for species distribution models: a methodological comparison. *Ecography*, *43*(1), pp.11-24.

Brown, C.R., Sergio, A.J., Bate, C.S., Koopman, N., Roland, J.B., Notman-Grobler, O.D., Mastrodimitropoulos, P.M., Piczak, M.L. and Lennox, R.J., 2025. A review of migratory Alosidae marine ecology in the northwest Atlantic. *Journal of Fish Biology*, *106*(3), pp.677-695.

Conley, E.D., Werner, S., Ardini, G., Cutler, M. and Clay, P.M., 2026. High Cost and Low Trust: Insights From Qualitative Commercial Fishing Cost Data in the Northeast United States. *Fisheries Management and Ecology*.

Cournane, J.M., Kritzer, J.P. and Correia, S.J., 2013. Spatial and temporal patterns of anadromous alosine bycatch in the US Atlantic herring fishery. *Fisheries Research*, *141*, pp.88-94.

Chen, C., Beardsley, R.C. and COWLES, G., 2006. An unstructured grid, finite-volume coastal ocean model (FVCOM) system. *Oceanography*, *19*(1), pp.78-89.

Davies, S.C., Thompson, P.L., Gomez, C., Nephin, J., Knudby, A., Park, A.E., Friesen, S.K., Pollock, L.J., Rubidge, E.M., Anderson, S.C. and Iacarella, J.C., 2023. Addressing uncertainty when projecting marine species' distributions under climate change. *Ecography*, *2023*(11), p.e06731.

Gahagan, B.I. and Bailey, M.M., 2020. Surgical implantation of acoustic tags in American Shad to resolve riverine and marine restoration challenges. *Marine and Coastal Fisheries*, *12*(5), pp.272-289

Hare, J.A., Borggaard, D.L., Alexander, M.A., Bailey, M.M., Bowden, A.A., Damon-Randall, K., Didden, J.T., Hasselman, D.J., Kerns, T., McCrary, R. and McDermott, S., 2021. A review of RHS science in support of species conservation and ecosystem restoration. *Marine and Coastal Fisheries*, *13*(6), pp.627-664.

Hijmans, R.J., Bivand, R., Dyba, K., Pebesma, E. and Sumner, M., 2023. Terra [R Package]. *R Programming Language*.

Kritzer, J.P., Hall, C.J., Hoppe, B., Ogden, C. and Cournane, J.M., 2022. Managing small fish at large scales: The emergence of regional policies for RHS in the eastern United States. *Fisheries*, *47*(10), pp.435-445.

Leggett, W.C., 1977. Ocean migration rates of American shad (Alosa sapidissima). *Journal of the Fisheries Board of Canada*, *34*(9), pp.1422-1426.

Lindgren, F., Rue, H. and Lindström, J., 2011. An explicit link between Gaussian fields and Gaussian Markov random fields: the stochastic partial differential equation approach. *Journal of the royal statistical society: Series b (statistical methodology)*, *73*(4), pp.423-498.

Lo, N.C.H., Jacobson, L.D. and Squire, J.L., 1992. Indices of relative abundance from fish spotter data based on delta-lognornial models. *Canadian Journal of Fisheries and Aquatic Sciences*, *49*(12), pp.2515-2526.

Millspaugh, J.J., Nielson, R.M., McDonald, L., Marzluff, J.M., Gitzen, R.A., Rittenhouse, C.D., Hubbard, M.W. and Sheriff, S.L., 2006. Analysis of resource selection using utilization distributions. *The Journal of Wildlife Management*, *70*(2), pp.384-395.

New England Fishery Management Council (NEFMC), 2014. Framework adjustment 3 to the Atlantic herring fishery management plan (FMP).

New England Fishery Management Council (NEFMC), 2016. Atlantic herring fishery specifications for the 2016-2018 fishing years.

New England Fishery Management Council (NEFMC), 2024. Atlantic herring fishery management plan scoping document for Amendment 10, February 16, 2024. pp. 1-18

New England Fishery Management Council (NEFMC), 2025. Atlantic herring fishery management 2025-2027 specifications, May 6, 2025. pp. 1-62.

Paradinas, I., Illian, J.B., Alonso-Fernández, A., Pennino, M.G. and Smout, S., 2023. Combining fishery data through integrated species distribution models. *ICES Journal of Marine Science*, *80*(10), pp.2579-2590.

R Core Team (2024). R: A Language and Environment for Statistical Computing. R Foundation for Statistical Computing, Vienna, Austria. <https://www.R-project.org/>.

Roberts, K.E., Stepanuk, J.E.F., Kim, H., Thorne, L.H., Chong-Montenegro, C. and Nye, J.A., 2023. Developing a subseasonal ecological forecast to reduce fisheries bycatch in the Northeast US. *Progress in Oceanography*, *213*, p.103021.

Rulifson, R.A. and Dadswell, M.J., 2020. Alewife and blueback herring captured by intertidal weirs of the inner Bay of Fundy, Canada, display seasonal demographics that suggest multiple migrating stocks. *Marine and Coastal Fisheries*, *12*(6), pp.441-456.

Thorson, J.T., Shelton, A.O., Ward, E.J. and Skaug, H.J., 2015. Geostatistical delta-generalized linear mixed models improve precision for estimated abundance indices for West Coast groundfishes. *ICES Journal of Marine Science*, *72*(5), pp.1297-1310.

Thorson, J.T., Adams, G. and Holsman, K., 2019. Spatio-temporal models of intermediate complexity for ecosystem assessments: A new tool for spatial fisheries management. *Fish and Fisheries*, *20*(6), pp.1083-1099.

Turner, S.M., Hare, J.A., Manderson, J.P., Richardson, D.E. and Hoey, J.J., 2017. Evaluation of species distribution forecasts: a potential predictive tool for reducing incidental catch in pelagic fisheries. *Canadian journal of fisheries and aquatic sciences*, *74*(11), pp.1717-1731.

Turner, S.M., Hare, J.A., Manderson, J.P., Hoey, J.J., Richardson, D.E., Sarro, C.L. and Silva, R., 2017. Cooperative research to evaluate an incidental catch distribution forecast. *Frontiers in Marine Science*, *4*, p.116.

Ward, E.J. and Anderson, S.C., 2025. Approximating spatial processes with too many knots degrades the quality of probabilistic predictions. *bioRxiv*, pp.2025-11.

Warren, D.L. and Seifert, S.N., 2011. Ecological niche modeling in Maxent: the importance of model complexity and the performance of model selection criteria. *Ecological applications*, *21*(2), pp.335-342.

Weatherall, P., Marks, K.M., Jakobsson, M., Schmitt, T., Tani, S., Arndt, J.E., Rovere, M., Chayes, D., Ferrini, V. and Wigley, R., 2015. A new digital bathymetric model of the world's oceans. *Earth and space Science*, *2*(8), pp.331-345.

Wood, S.N., 2017. *Generalized additive models: an introduction with R*. chapman and hall/CRC.

Tables

Table 1. Number of hauls and percent occurrence for each dataset used to fit species distribution models.

			% Occurrence (2000-2023)			
Dataset	Available Years	Hauls (2000-2023)	Alewife	Blueback Herring	American Shad	Atlantic Herring
MENH	2000-present	3937	89	51	41	79
SHRIMP	1983-2023	1441	36	7	8	74
IBS	2003-2007; 2016-2019	3466	67	17	23	63
MADMF	1978-present	4249	19	7	7	16
RIDEM	1980-present	4510	29	13	8	29
CTLISTS	1984-present	3947	28	11	25	21
NJOT	1988-present	1594	57	64	44	75
NEAMAP	2007-present	3496	23	22	25	9
NEFSC	1963-present	16032	22	10	7	26
OBS_SMBT	1994-present	36311	11	5	12	12
OBS_MWT	1994-present	2475	15	12	6	93

MENH = Maine-New Hampshire Inshore Trawl Survey; SHRIMP = ASMFC Summer Shrimp Survey; IBS = Industry-Based Survey for GOM Cod; MADMF = Massachusetts Resource Assessment Trawl Survey; RIDEM = Rhode Island Coastal Trawl Survey; CTLISTS = Connecticut Long Island Sound Trawl Survey; NJOT = New Jersey Ocean Trawl Survey; NEAMAP = Northeast Area Monitoring and Assessment Program; NEFSC = Northeast Fisheries Science Center Bottom Trawl Survey; OBS_SMBT = Fishery Observers - Small-Mesh Bottom Trawl; OBS_MWT = Fishery Observers - Midwater Trawl.

Table 2. Candidate variables used in model selection.

Variable	Alewife	Blueback Herring	American Shad	Atlantic Herring
main effects				
SOURCE	X	X	X	X
(1|YEAR)	X	X	X	X
s(J*)				
s(H*)				
s(DEPTH)		X		
s(DSHORE)				
s(BOTTEMP)	X			
s(SURFTEMP)	X	X		X
s(BOTSALIN)				
s(SURFSALIN)				
s(DEPTH,J*)	X		X	X
s(DSHORE,J*)			X	
s(BOTTEMP,J*)		X		X
s(SURFTEMP,J*)			X	
s(BOTSALIN,J*)				
s(SURFSALIN,J*)	X			
spatiotemporal				
YEAR (ar1)				
MONTH (ar1)	X	X	X	X

An "X" indicates a variable was included in the selected model for that species. SOURCE = survey/fishery dataset, as factor (see table 1); (1|YEAR) = year as factor, treated as a random effect; J = day of year; H = hour of day; DEPTH = recorded depth at haul start; DSHORE = distance from shore at haul midpoint; BOTTEMP = recorded or expected bottom temperature; SURFTEMP = recorded or expected surface temperature; BOTSALIN = recorded or expected bottom salinity; SURFSALIN = recorded or expected surface salinity; SEASON = quarter of year, as factor; YEAR (ar1) = year, with 1st order auto-regressive correlation; MONTH (ar1) = month, with 1st order auto-regressive correlation. Variables with s(_) were treated as non-linear smoothers. Variables with an "*" were treated as circular variables where the effect at min and max values are identical. Variables with s(_,J*) are 2D smoothers that vary seasonally.

Table 3. Forward selection of candidate models. Beginning with a naïve model (~ 1; intercept only, with a spatial random field), each additional row shows the BIC, ΔBIC (i.e., change in BIC from previous row), and EDF (equivalent degrees of freedom) resulting from the inclusion of the next best-fitting term. Once the optimal fixed effects were selected, the spatial random field was allowed to vary over time, either by month or year. The final select model for each species is shown in bold.

Fixed Effects	Random Fields	BIC	ΔBIC	EDF
Alewife				
~ 1	spatial	263014		7
~ s(DEPTH,J*)	spatial	255264	-7750	9
~ s(DEPTH,J*) + s(SURFTEMP)	spatial	254359	-906	13
~ s(DEPTH,J*) + s(SURFTEMP) + SOURCE	spatial	251658	-2700	33
~ s(DEPTH,J*) + s(SURFTEMP) + SOURCE + s(SURFSALIN,J*)	spatial	250650	-1008	35
~ s(DEPTH,J*) + s(SURFTEMP) + SOURCE + s(SURFSALIN,J*) + (1|YFAC)	spatial	249899	-751	37
~ s(DEPTH,J*) + s(SURFTEMP) + SOURCE + s(SURFSALIN,J*) + (1|YFAC) + s(BOTTEMP)	spatial	249787	-112	41
~ s(DEPTH,J*) + s(SURFTEMP) + SOURCE + s(SURFSALIN,J*) + (1|YFAC) + s(BOTTEMP)	**spatiotemporal - MONTH (AR1)**	**245082**	**-4706**	**43**
~ s(DEPTH,J*) + s(SURFTEMP) + SOURCE + s(SURFSALIN,J*) + (1|YFAC) + s(BOTTEMP)	spatiotemporal - YEAR (AR1)	247616	+2534	43
Blueback herring				
~ 1	spatial	130143		7
~ 1 + s(BOTTEMP,J*)	spatial	125279	-4864	9
~ 1 + s(BOTTEMP,J*) + SOURCE	spatial	122171	-3108	29
~ 1 + s(BOTTEMP,J*) + SOURCE + (1|YFAC)	spatial	121756	-415	31
~ 1 + s(BOTTEMP,J*) + SOURCE + (1|YFAC) + s(SURFTEMP)	spatial	121469	-286	35
~ 1 + s(BOTTEMP,J*) + SOURCE + (1|YFAC) + s(SURFTEMP) + s(DEPTH)	spatial	121361	-108	39
~ 1 + s(BOTTEMP,J*) + SOURCE + (1|YFAC) + s(SURFTEMP) + s(DEPTH)	**spatiotemporal - MONTH (AR1)**	**119224**	**-2138**	**43**
~ 1 + s(BOTTEMP,J*) + SOURCE + (1|YFAC) + s(SURFTEMP) + s(DEPTH)	spatiotemporal - YEAR (AR1)	119858	+634	43

Table 3 (Continued)

Fixed Effects	Random Fields	BIC	ΔBIC	EDF
American shad				
~ 1	spatial	144470		7
~ s(DEPTH,J*)	spatial	141835	-2635	11
~ s(DEPTH,J*) + SOURCE	spatial	140283	-1552	29
~ s(DEPTH,J*) + SOURCE + (1|YFAC)	spatial	139518	-765	31
~ s(DEPTH,J*) + SOURCE + (1|YFAC) + s(SURFTEMP,J*)	spatial	139193	-325	33
~ s(DEPTH,J*) + SOURCE + (1|YFAC) + s(SURFTEMP,J*) + s(DSHORE,J*)	spatial	138916	-277	35
~ s(DEPTH,J*) + SOURCE + (1|YFAC) + s(SURFTEMP,J*) + s(DSHORE,J*)	**spatiotemporal - MONTH (AR1)**	**136219**	**-2697**	**39**
~ s(DEPTH,J*) + SOURCE + (1|YFAC) + s(SURFTEMP,J*) + s(DSHORE,J*)	spatiotemporal - YEAR (AR1)	137136	+917	39
Atlantic herring				
~ 1	spatial	357839		7
~ SOURCE	spatial	344881	-12958	27
~ SOURCE + s(BOTTEMP,J*)	spatial	338489	-6391	29
~ SOURCE + s(BOTTEMP,J*) + (1|YFAC)	spatial	337130	-1360	31
~ SOURCE + s(BOTTEMP,J*) + (1|YFAC) + s(DEPTH,J*)	spatial	336657	-473	33
~ SOURCE + s(BOTTEMP,J*) + (1|YFAC) + s(DEPTH,J*) + s(SURFTEMP)	spatial	336334	-324	37
~ SOURCE + s(BOTTEMP,J*) + (1|YFAC) + s(DEPTH,J*) + s(SURFTEMP)	**spatiotemporal - MONTH (AR1)**	**330233**	**-6101**	**41**
~ SOURCE + s(BOTTEMP,J*) + (1|YFAC) + s(DEPTH,J*) + s(SURFTEMP)	spatiotemporal - YEAR (AR1)	333375	3142	41

Table 4. Evaluation of hypothetical closure scenarios using observed fishery hauls, by gear.

Midwater Trawl

Min RHS Biomass Quantile	RHS CPUE (Kg / Km2)			Atlantic Herring CPUE (Kg / Km2)			% of Total Catch Inside Closure	
	Closed	Open	% Diff	Closed	Open	% Diff	RHS	Atl Herring
0.1	333	2	+19091%	65,061	56,765	-15%	99%	50%
0.2	368	4	+8833%	67,133	55,871	-20%	99%	45%
0.3	393	16	+2325%	70,434	54,561	-29%	93%	41%
0.4	392	30	+1186%	70,009	55,381	-26%	89%	39%
0.5	416	37	+1018%	72,275	54,982	-31%	86%	36%
0.6	433	72	+505%	74,956	55,882	-34%	74%	28%
0.7	536	87	+517%	73,146	58,252	-26%	63%	19%
0.8	603	109	+454%	77,603	58,678	-32%	44%	13%
0.9	952	138	+589%	74,482	60,409	-23%	22%	4%

Bottom Trawl

Min RHS Biomass Quantile	RHS CPUE (Kg / Km2)			Atlantic Herring CPUE (Kg / Km2)			% of Total Catch Inside Closure	
	Closed	Open	% Diff	Closed	Open	% Diff	RHS	Atl Herring
0.1	226	12	+1783%	7,191	316	-2173%	99%	99%
0.2	246	63	+291%	8,474	790	-973%	91%	97%
0.3	308	71	+331%	10,793	1,383	-680%	84%	89%
0.4	375	78	+379%	12,544	2,138	-487%	76%	77%
0.5	420	86	+391%	13,587	2,610	-421%	68%	69%
0.6	492	90	+446%	15,266	2,947	-418%	63%	61%
0.7	512	99	+418%	16,231	3,132	-418%	58%	57%
0.8	596	115	+419%	16,285	4,040	-303%	46%	40%
0.9	1,407	157	+795%	15,331	5,514	-178%	9%	3%

Closure scenarios were based on the minimum RHS biomass quantile (Figure 16). For both RHS and Atlantic Herring, the average catch rate (CPUE) inside and outside of a closure scenario is listed, as is the percent difference ([closed-open]/open). The last two columns show the fraction of the total catch of RHS and Atlantic Herring encompassed by the closure scenario. Hauls that occurred inside any existing closure (Figure 6) were excluded.

Figures

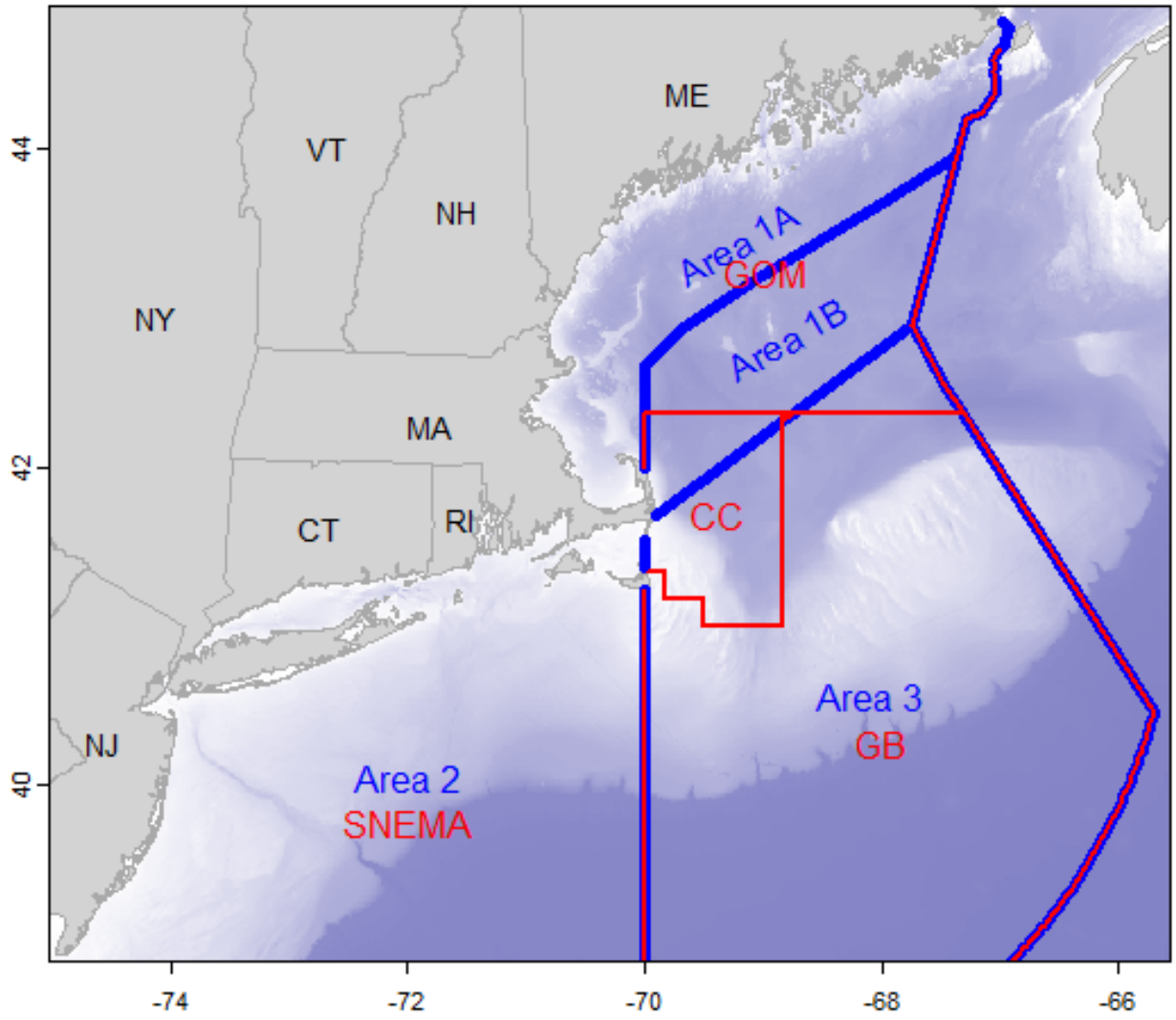


Figure 1. Map of management areas (thick blue lines), and river herring catch cap areas (thin red lines) under the NEFMC Atlantic herring fishery management plan.

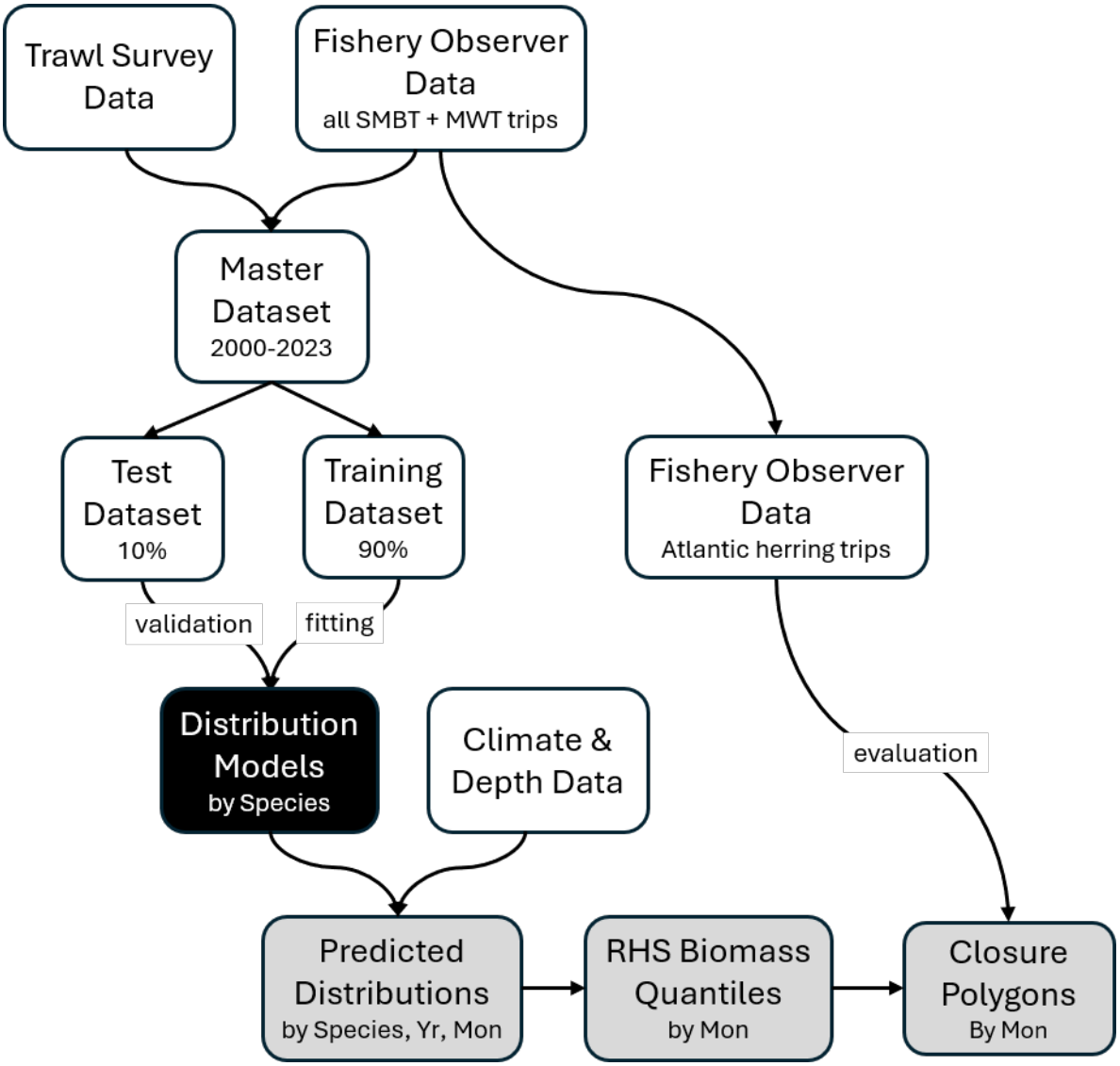


Figure 2. Conceptual diagram of how data (white boxes) were used to inform models (black box), from which predictions and closure polygons were derived (gray boxes).

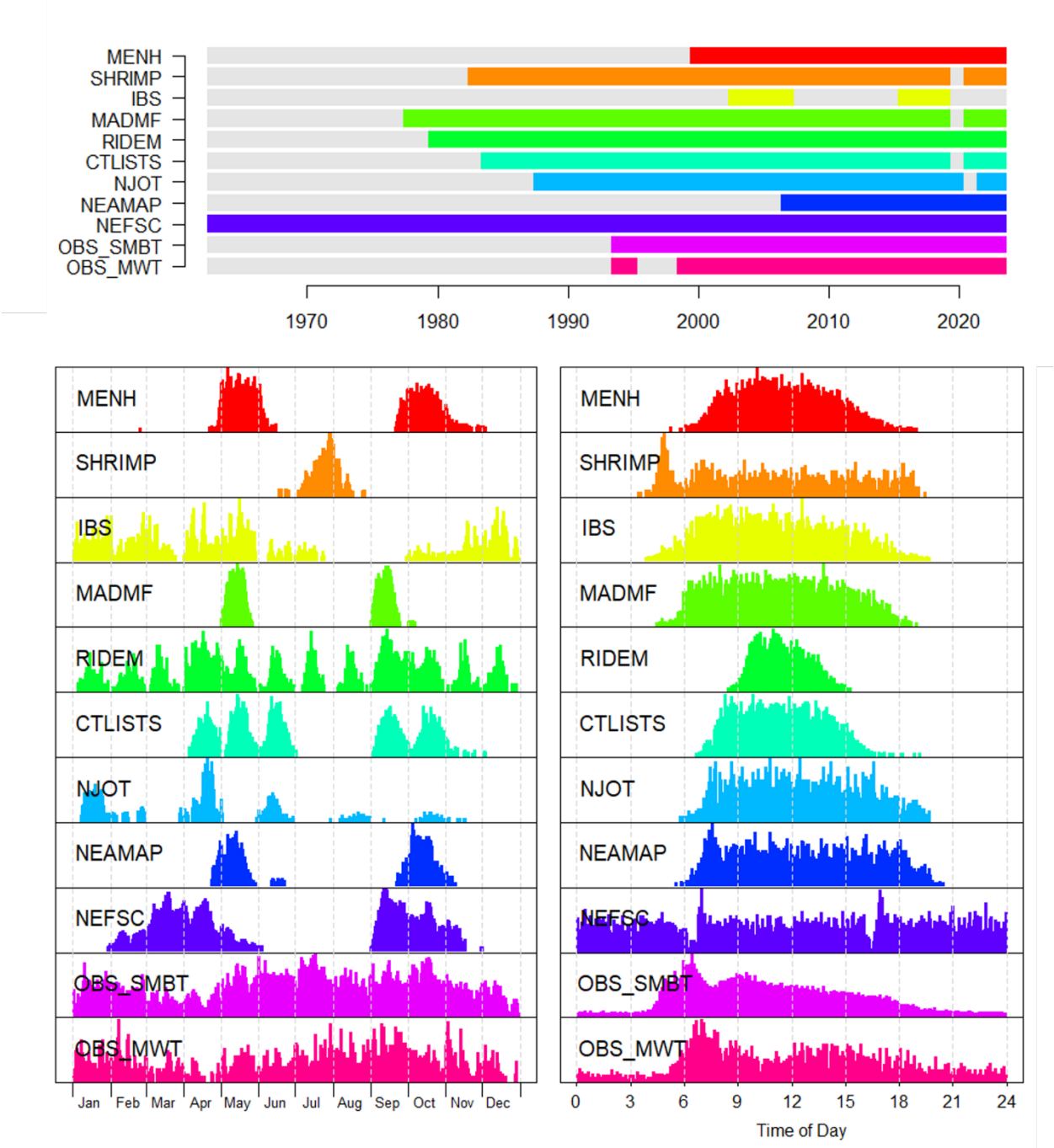


Figure 3. Interannual (top), seasonal (left), and diel (right) extents of the trawl survey and fishery observer datasets. Seasonal and diel distributions were limited to only the years used to fit models: 2000-2023.

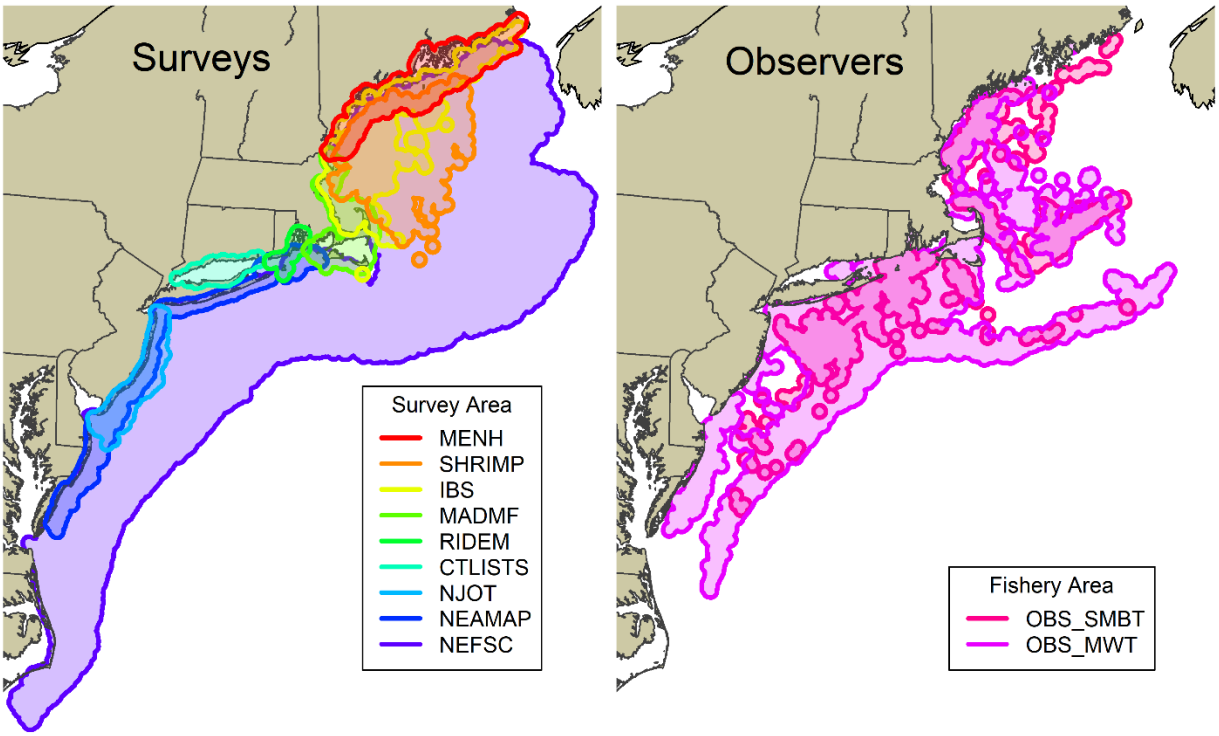


Figure 4. Spatial extent of bottom trawl survey (left) and fishery observer datasets (right).

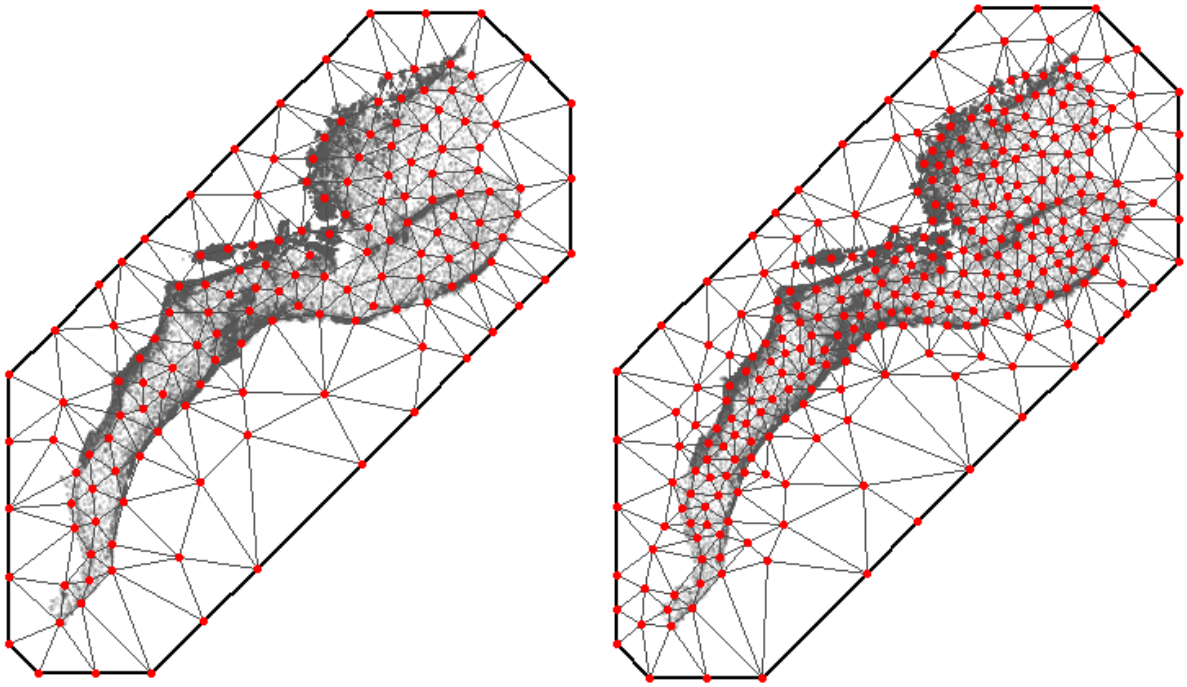


Figure 5. Triangular mesh used for spatial random effects in model selection (left; n = 150 knots) and for final model fitting (right; n = 300 knots).

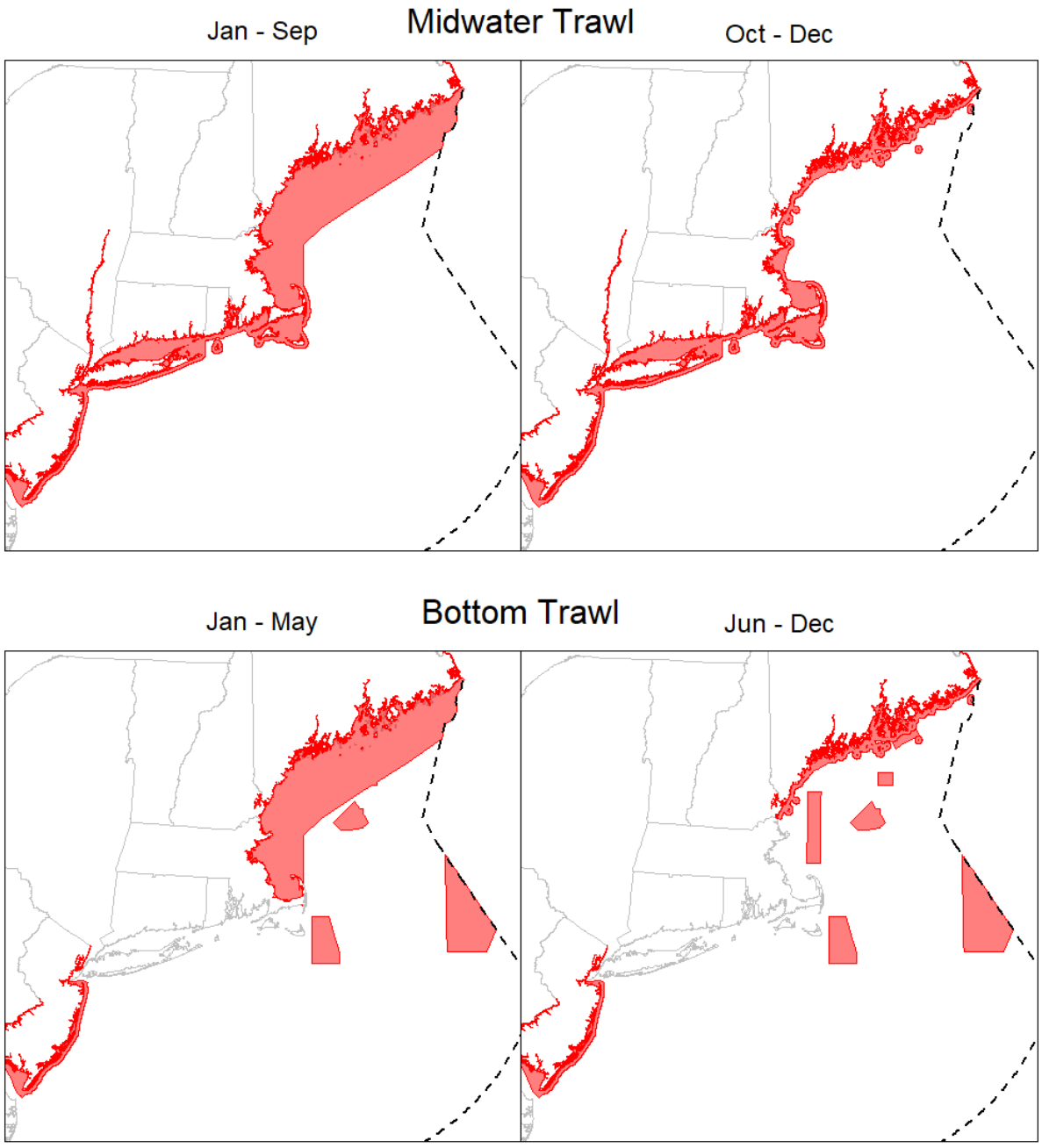


Figure 6. Current season-area restrictions on the Atlantic Herring fishery, by gear type (red areas indicate no access).

Per the ASMFC Atlantic Herring FMP, no quota is allocated to Herring Management Area 1A between Jan and May, and midwater trawls are prohibited from Area 1A until October. Midwater trawls are also prohibited from all state waters from ME to NJ, either explicitly or through vessel size restrictions. Bottom trawls are prohibited from the state waters of ME, NH, and NJ, as well as from groundfish and habitat management closed areas.

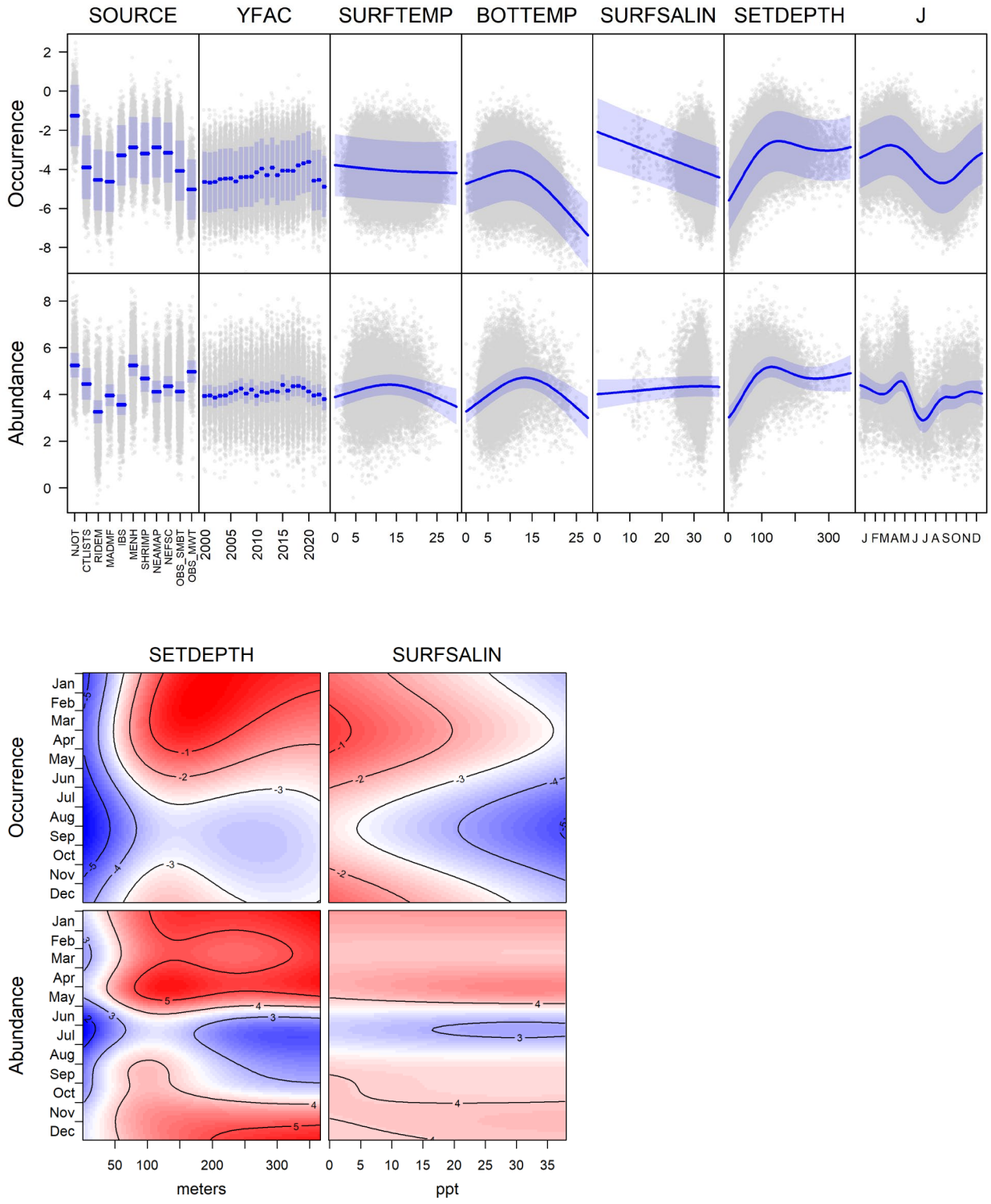


Figure 7. 1D (top) and 2D (bottom) marginal effects of predictors in the selected Alewife model. For the 2D plots, red = higher density and blue = lower density.

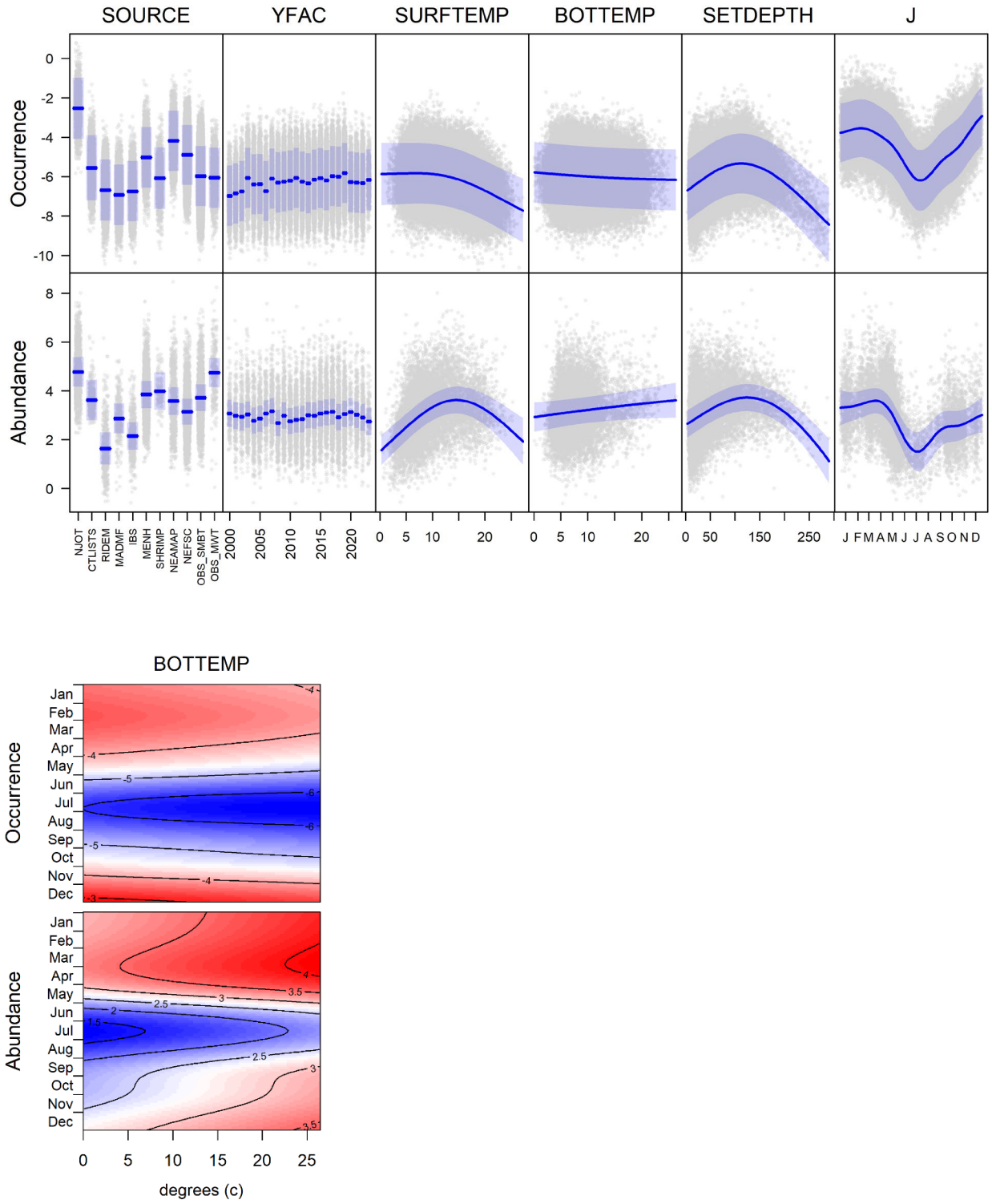


Figure 8. 1D (top) and 2D (bottom) marginal effects of predictors in the selected model for Blueback Herring. For the 2D plots, red = higher density and blue = lower density.

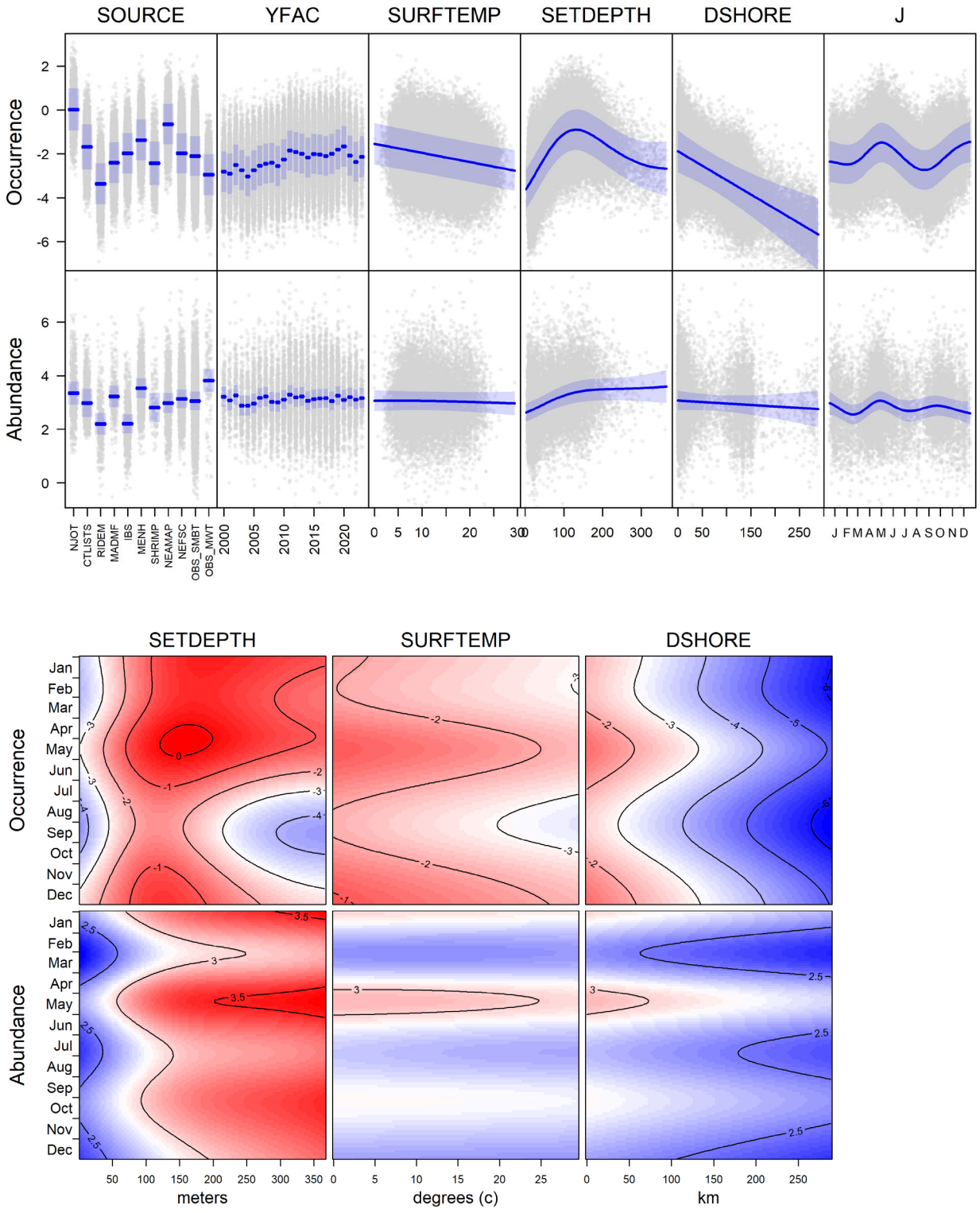


Figure 9. 1D (top) and 2D (bottom) marginal effects of predictors in the selected model for American Shad. For the 2D plots, red = higher density and blue = lower density.

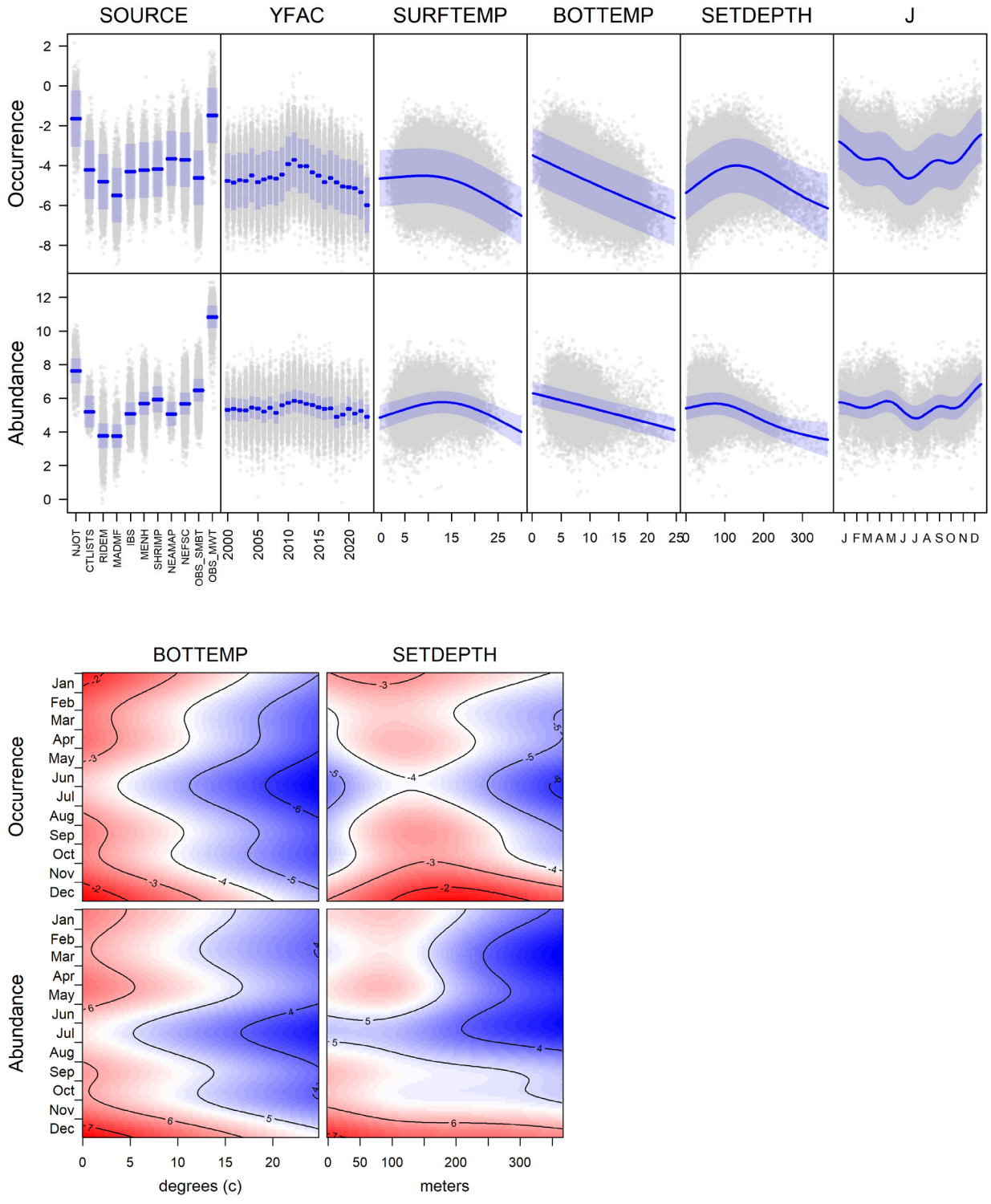


Figure 10. 1D (top) and 2D (bottom) marginal effects of predictors in the selected model for Atlantic Herring. For the 2D plots, red = higher density and blue = lower density.

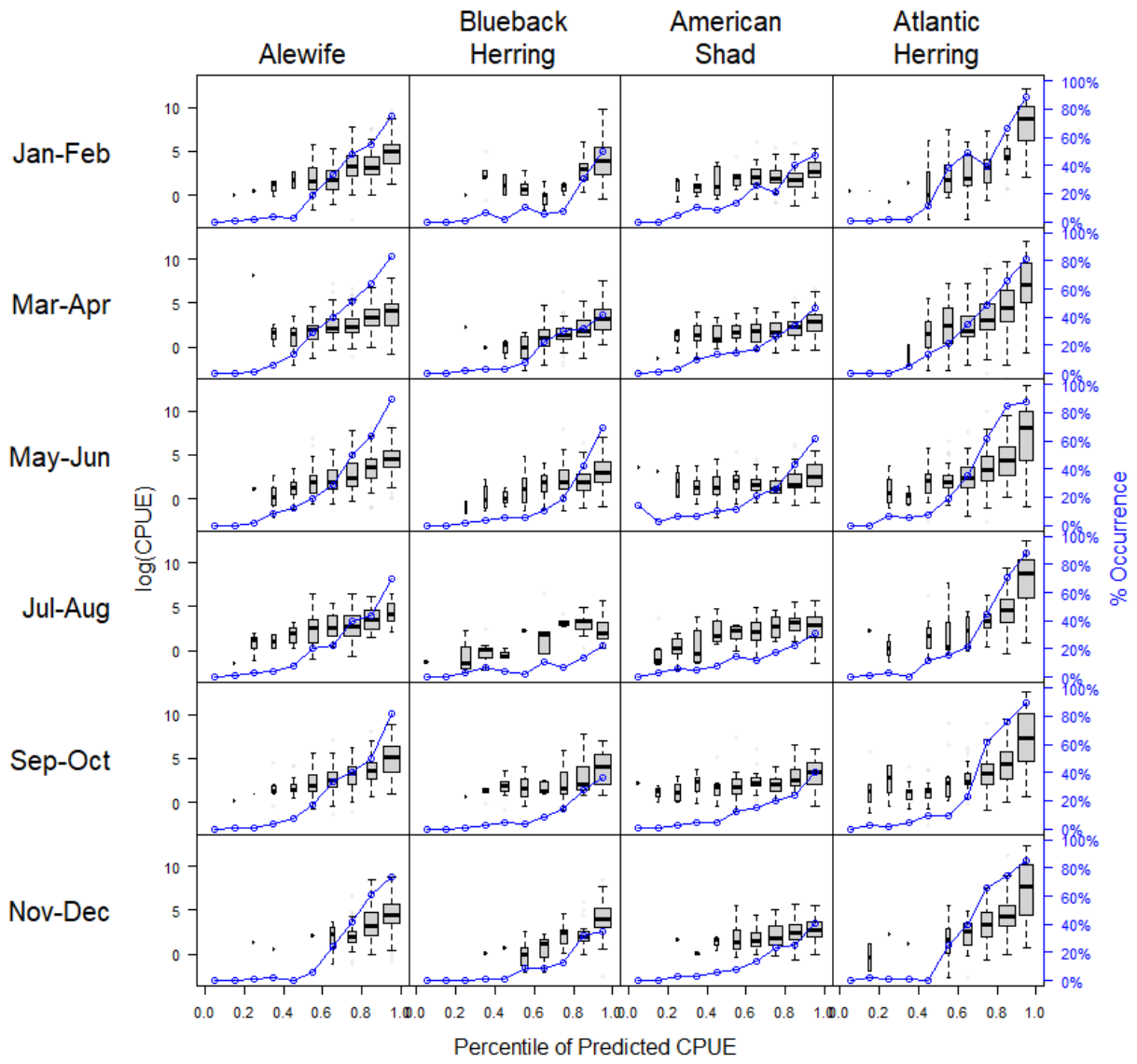


Figure 11. Observed log(CPUE) (boxplots) and percent occurrence (blue lines) from the test dataset (n = 8,141 hauls) grouped by 10-percentile bins of predicted CPUE from the species distribution models.

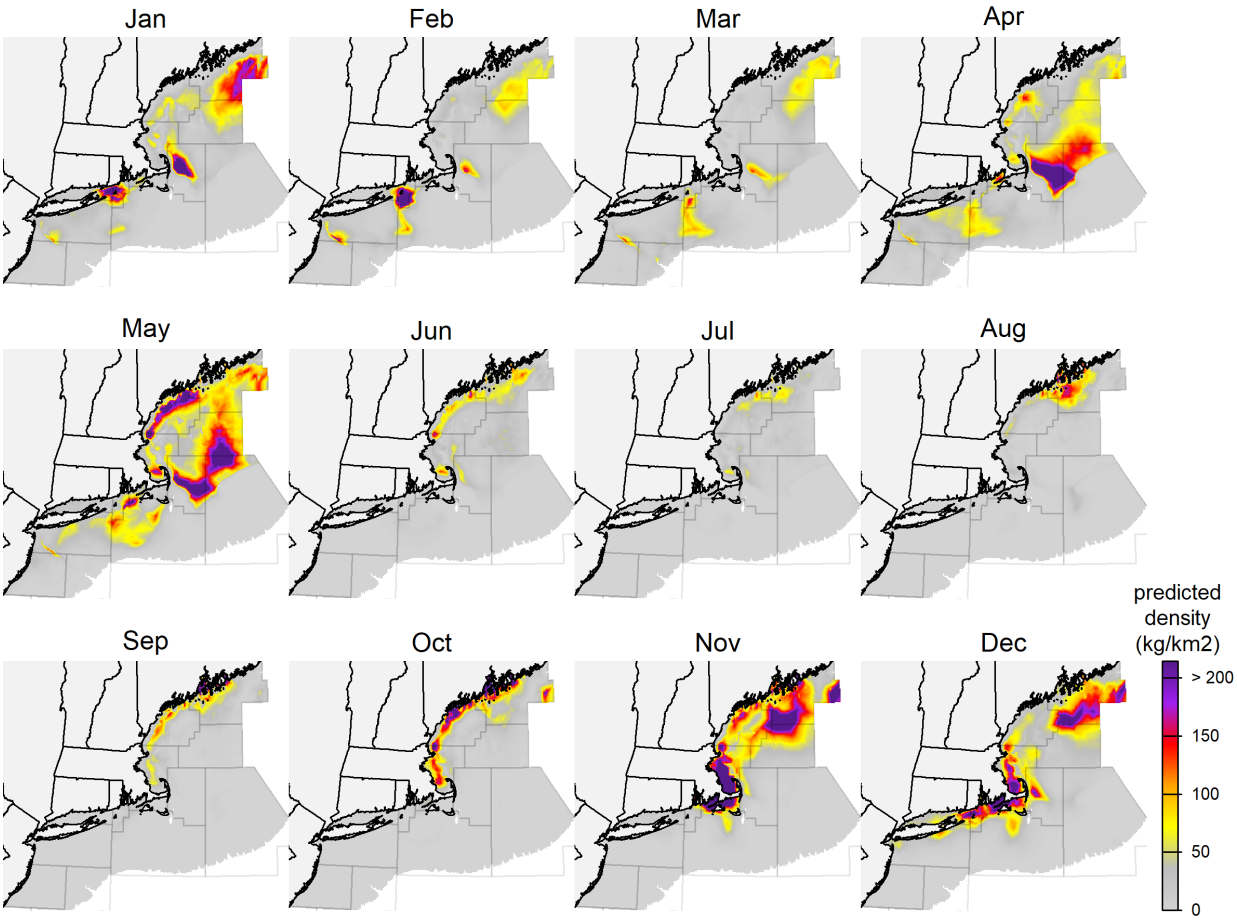


Figure 12. Predicted monthly distribution of alewife. Red and purple represent higher density areas, whereas yellow and gray represent the lower density areas.

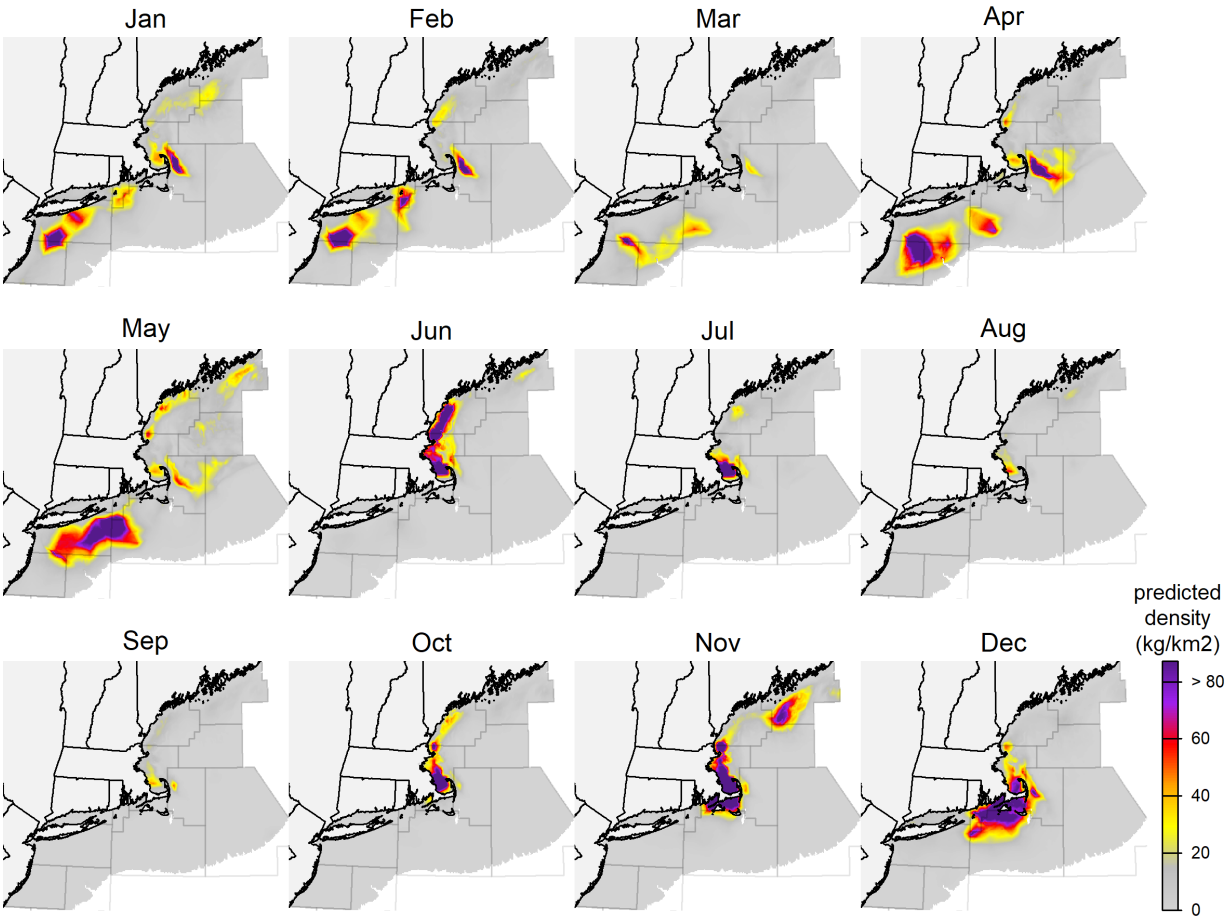


Figure 13. Predicted monthly distribution of blueback herring. Red and purple represent higher density areas, whereas yellow and gray represent the lower density areas

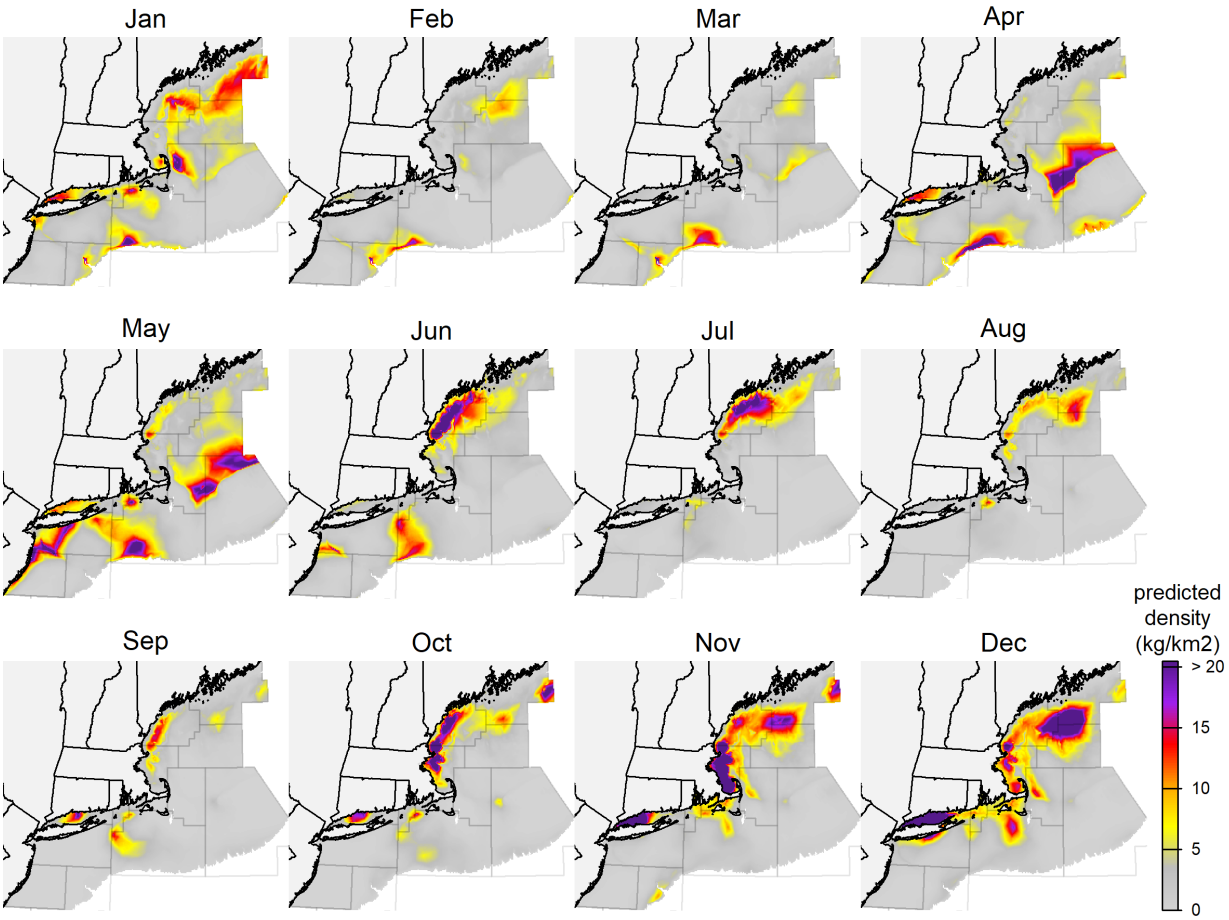


Figure 14. Predicted monthly distribution of American shad. Red and purple represent higher density areas, whereas yellow and gray represent the lower density areas

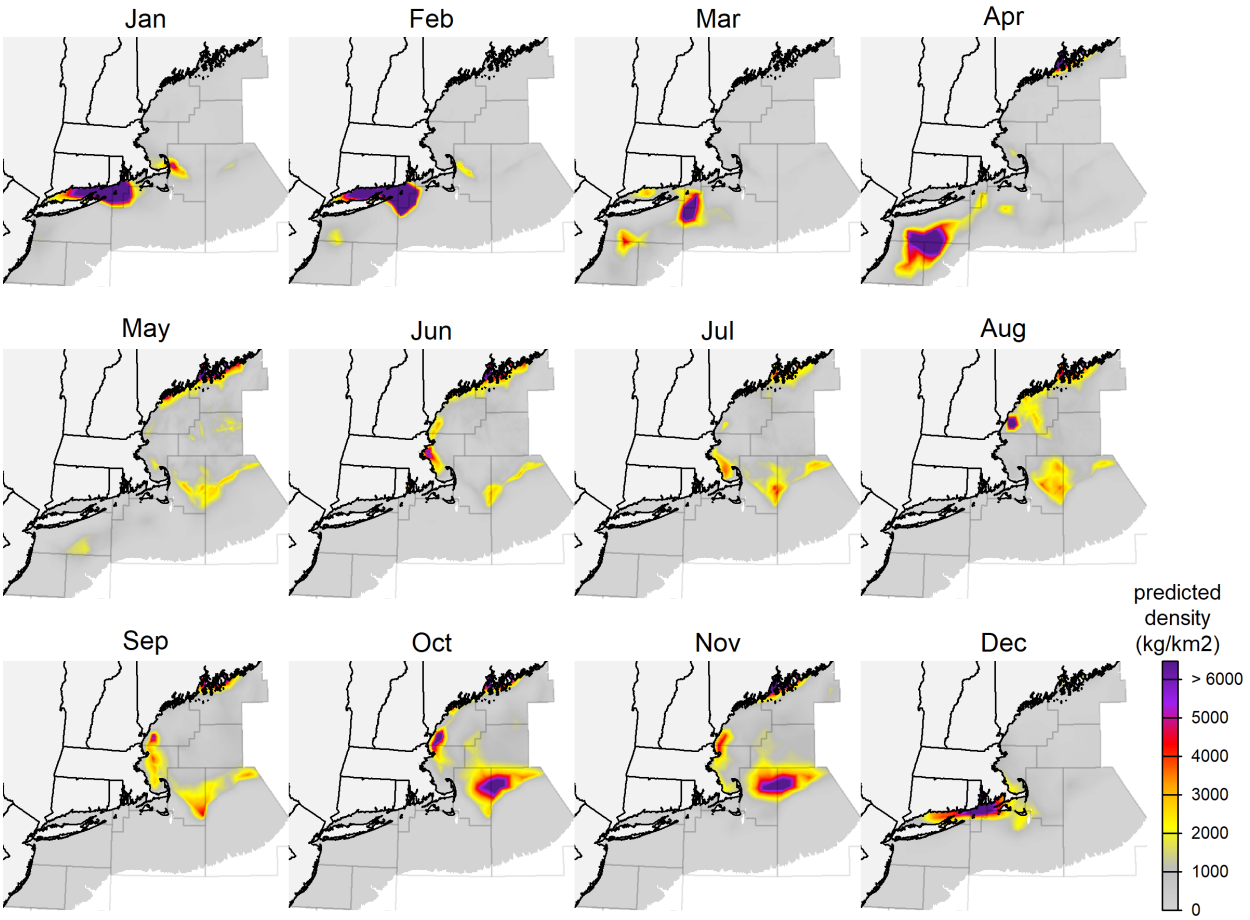


Figure 15. Predicted monthly distribution of Atlantic herring. Red and purple represent higher density areas, whereas yellow and gray represent the lower density areas

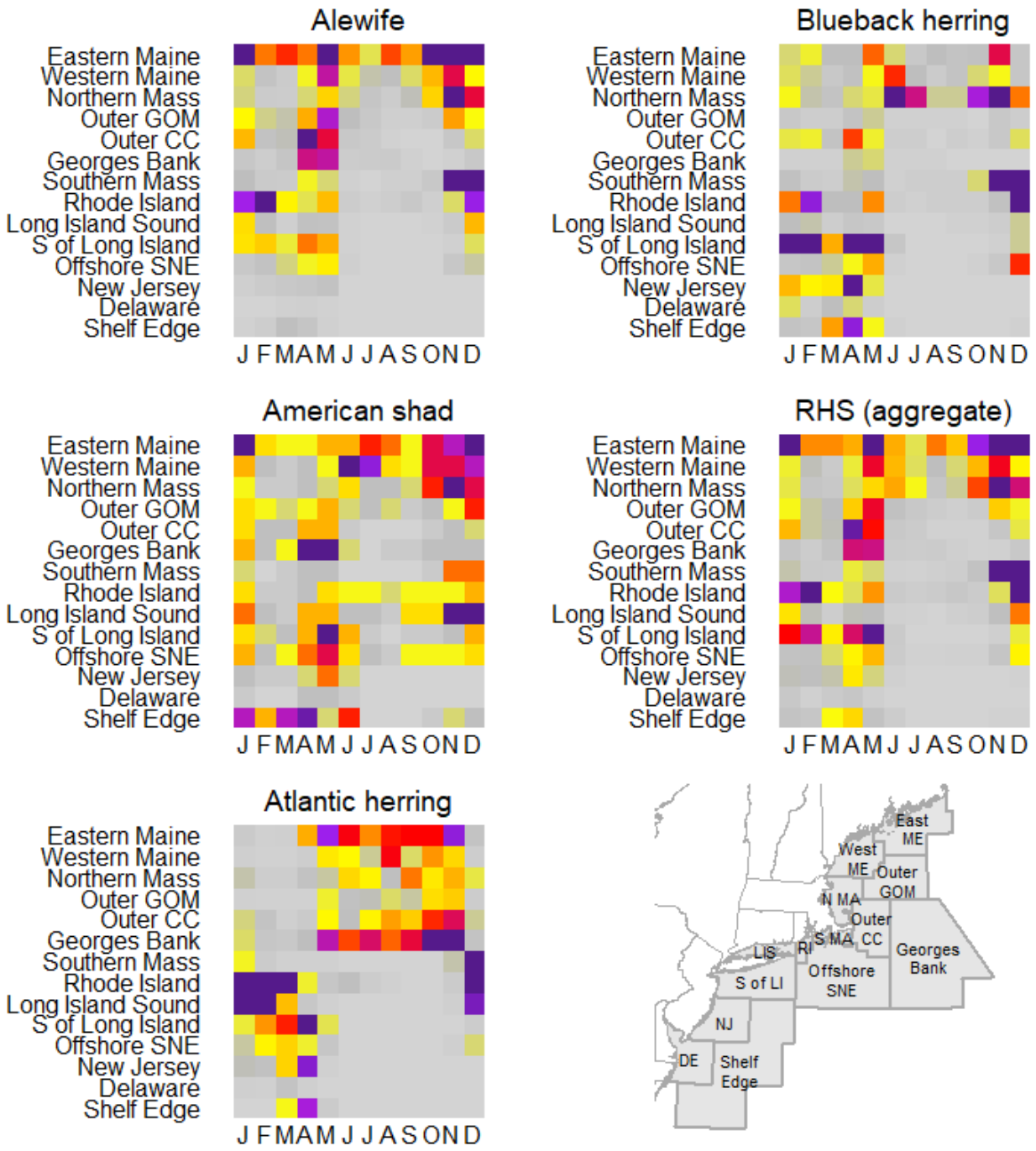


Figure 16. Average predicted monthly density (from Figures 12-16), by labeled groups of NOAA statistical reporting areas (bottom right). Red and purple represent higher densities, whereas yellow and gray represent lower densities.

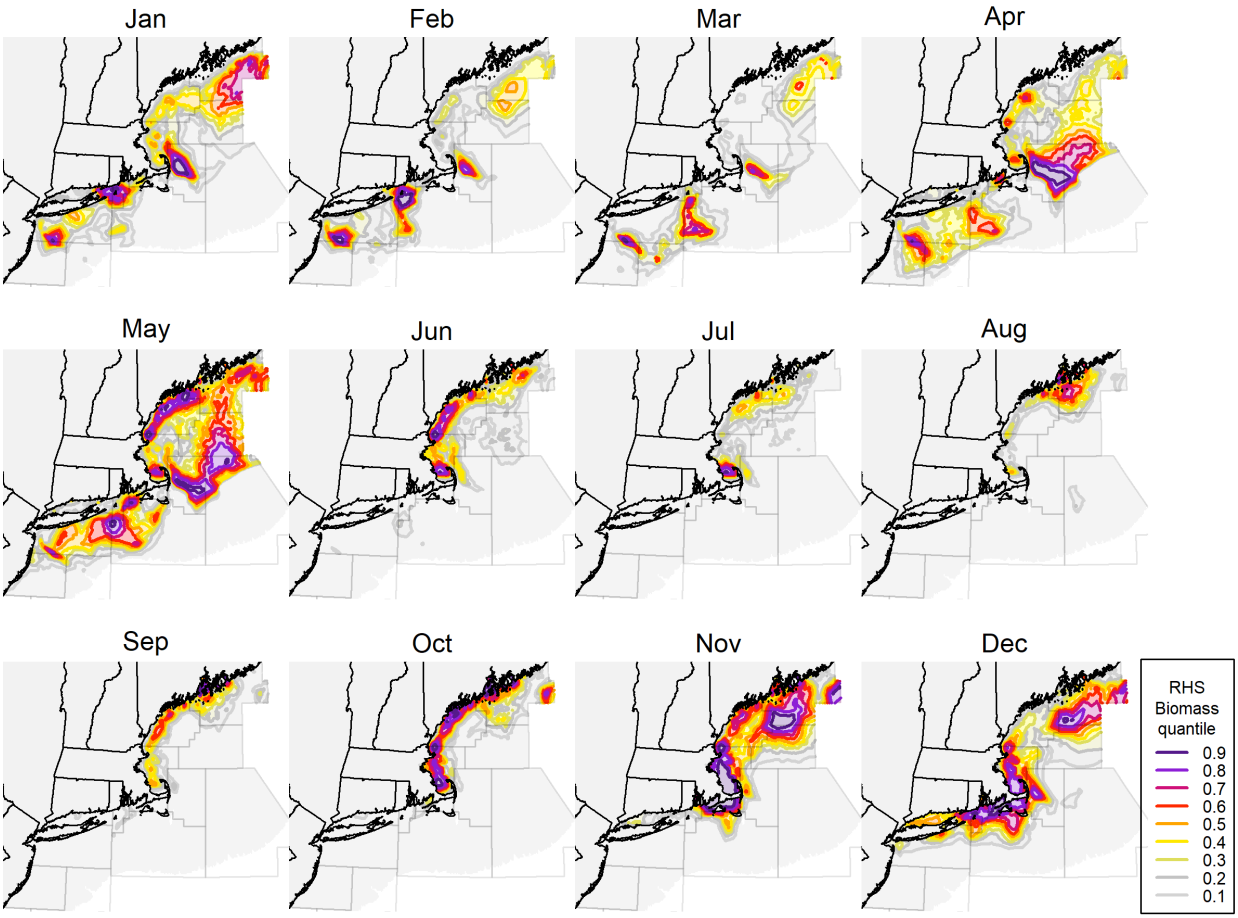


Figure 17. Predicted average biomass quantiles for all RHS species combined. Dark red and purple contour lines represent higher quantiles that encompass the areas of greatest density (e.g., the 0.9 quantile contour delineates the smallest area that encompasses 10% of the biomass).

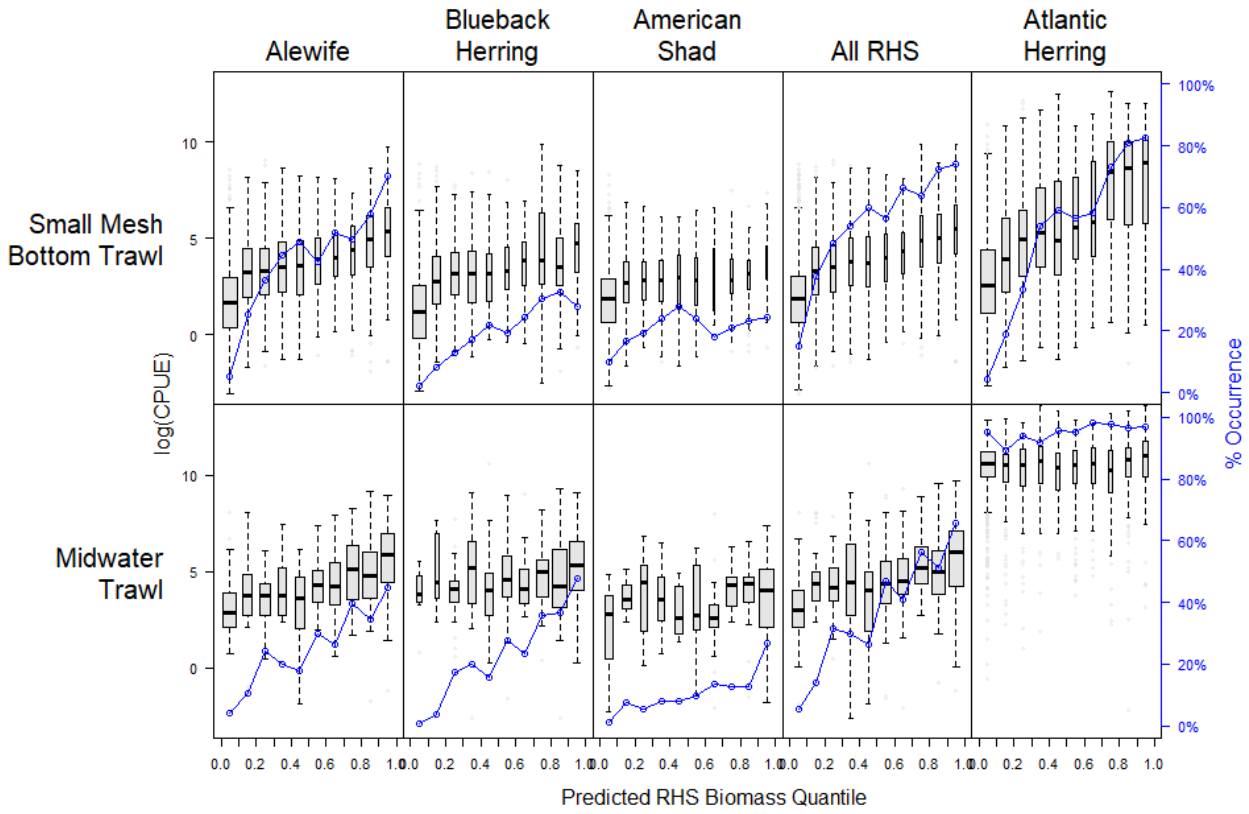


Figure 18. Observed log(CPUE) (boxplots) and percent occurrence (blue lines) from fishery hauls (SMBT: n = 36311; MWT; n = 2475), as compared to the average biomass quantile from the predicted RHS rasters.

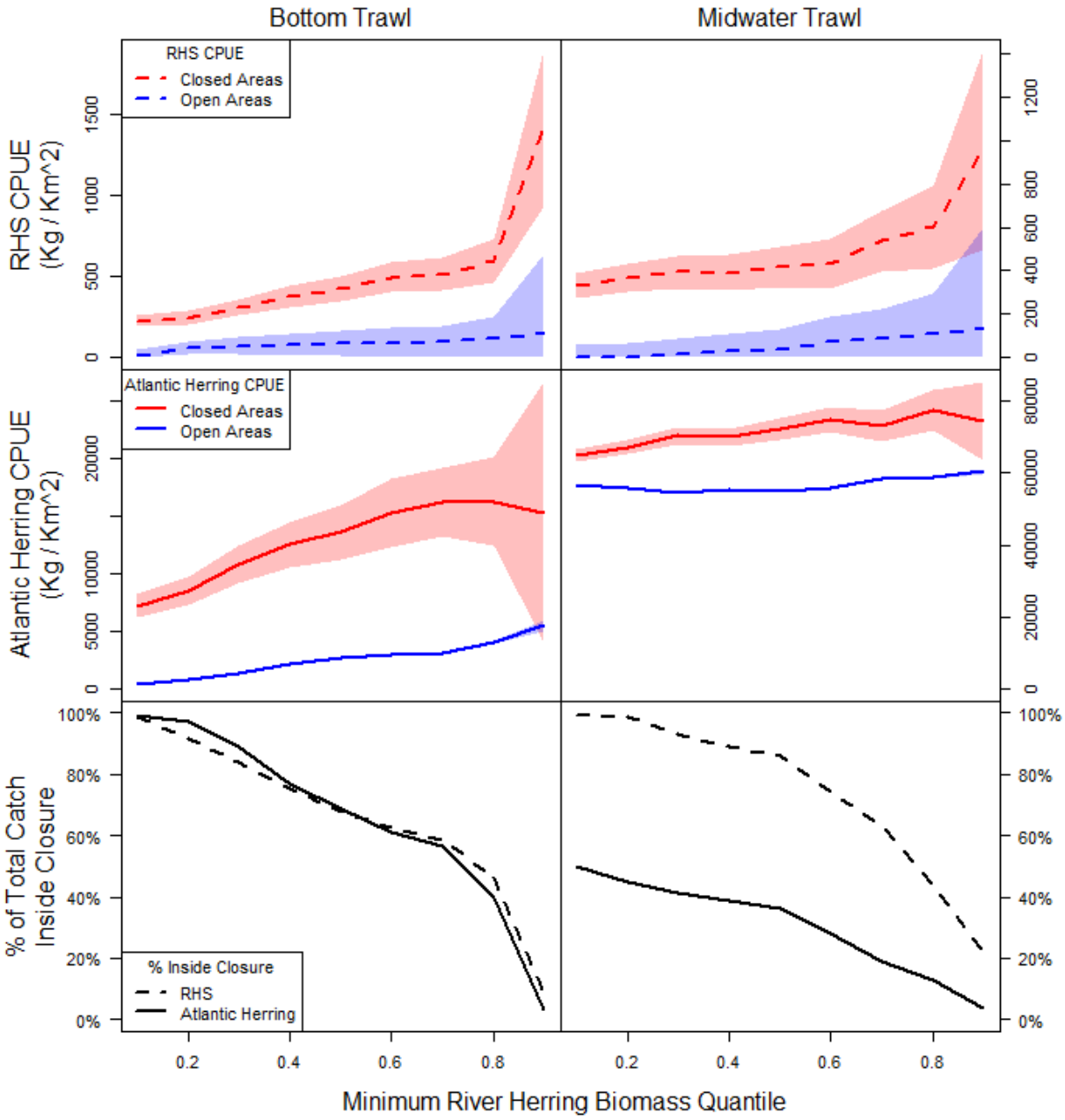


Figure 19. Comparison of catch rates for RHS species (top row) and Atlantic Herring (middle row) from all observed fishery hauls inside (red) and outside (blue) of closure scenarios based on the predicted minimum RHS biomass quantile (Figure 17). The bottom row shows the percent of total observed RHS catch (dashes), and of total Atlantic Herring catch (solid lines) encompassed by the closure scenarios. Any observed hauls from 2000-2023 with recorded Atlantic Herring landings were included. Hauls that occurred inside any existing closure (Figure 6) were excluded. The values shown in this figure are also available in Table 4.

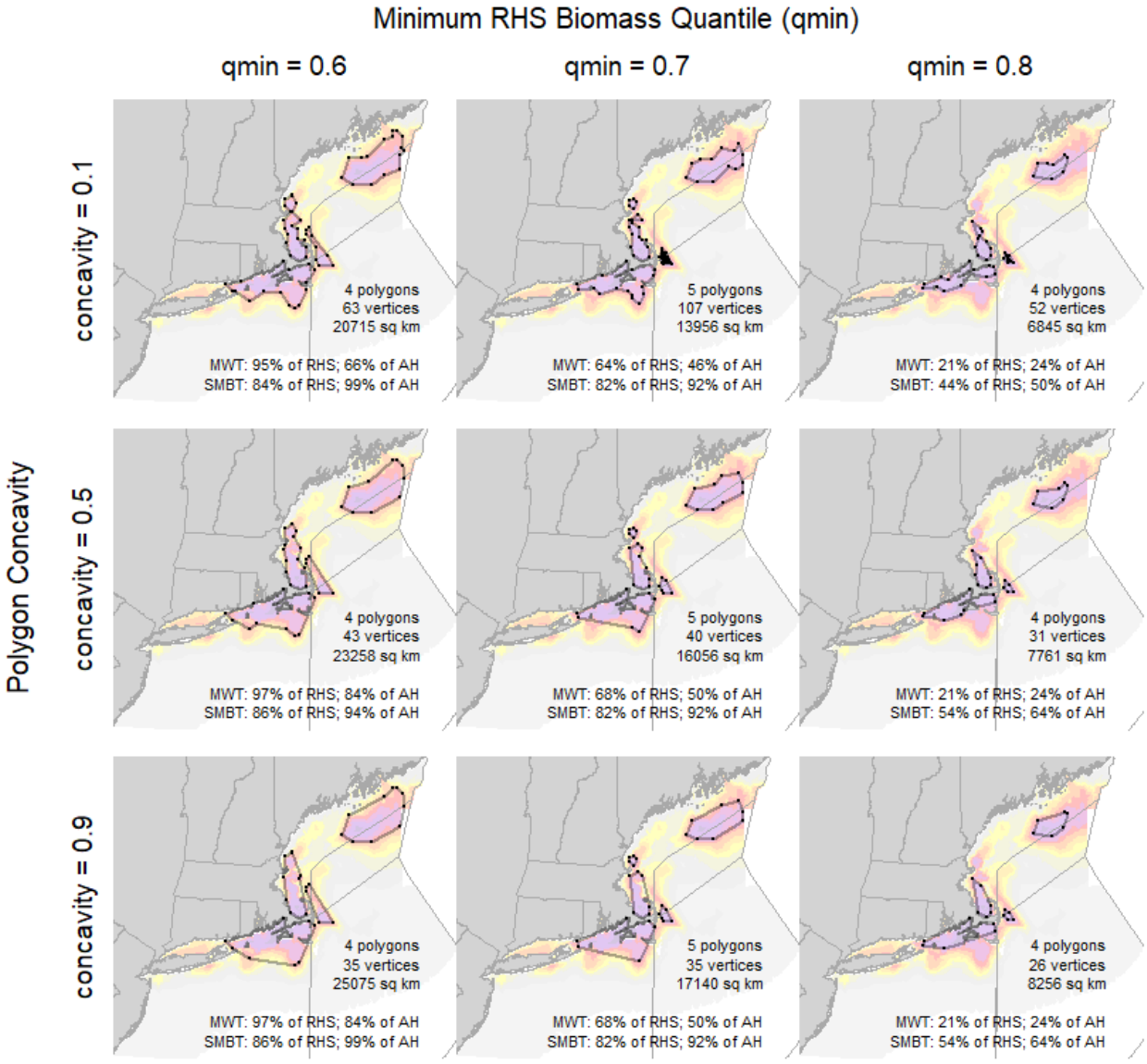


Figure 20. Hypothetical versions of closure polygons for the month of December, created by varying the minimum RHS biomass quantile (q_{min}, columns) and the polygon concavity threshold (rows). The background colorscale depicts the RHS biomass quantile raster for December (from figure 16). For each combination, the number of polygons, vertices, and spatial extent of the closure is provided, as is the percentage of total observed RHS and Atlantic herring (AH) encompassed by the closure polygons.